

# Journal Pre-proof

Pre-intercalation: A valuable approach for the improvement of post-lithium battery materials

Charlie A.F. Nason, Yang Xu



PII: S2667-1417(23)00123-4

DOI: <https://doi.org/10.1016/j.esci.2023.100183>

Reference: ESCI 100183

To appear in: *eScience*

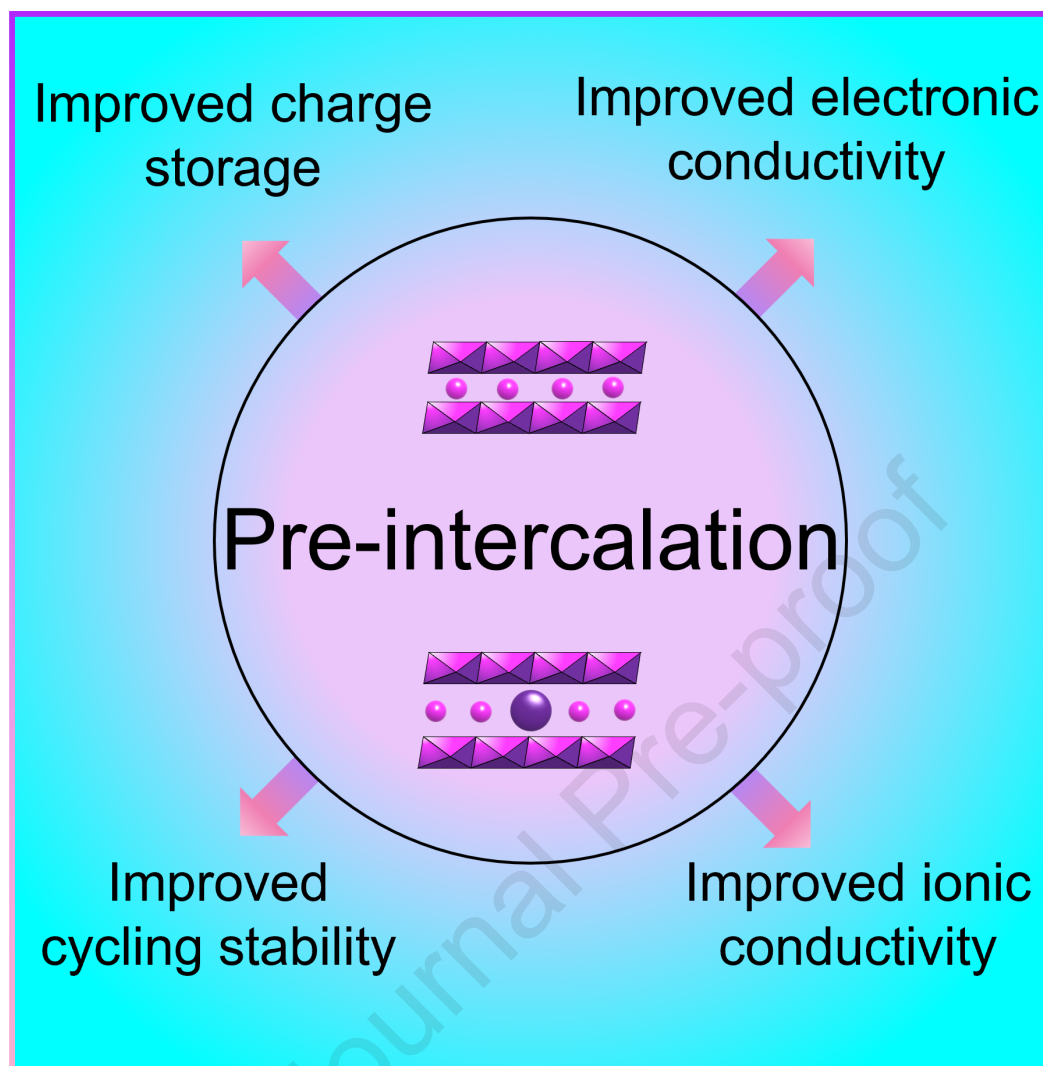
Received Date: 23 May 2023

Accepted Date: 1 September 2023

Please cite this article as: C.A.F. Nason, Y. Xu, Pre-intercalation: A valuable approach for the improvement of post-lithium battery materials, *eScience*, <https://doi.org/10.1016/j.esci.2023.100183>.

This is a PDF file of an article that has undergone enhancements after acceptance, such as the addition of a cover page and metadata, and formatting for readability, but it is not yet the definitive version of record. This version will undergo additional copyediting, typesetting and review before it is published in its final form, but we are providing this version to give early visibility of the article. Please note that, during the production process, errors may be discovered which could affect the content, and all legal disclaimers that apply to the journal pertain.

© 2023 The Authors. Published by Elsevier B.V. on behalf of Nankai University.



# Pre-intercalation: A valuable approach for the improvement of post-lithium battery materials

Charlie A. F. Nason<sup>1</sup> and Yang Xu<sup>1</sup>

<sup>1</sup> *Department of Chemistry, University College London, London, WC1H 0AJ, UK*

*Email: y.xu.1@ucl.ac.uk*

## Abstract

With the growing concern around the sustainability and supply of lithium, the need for alternative rechargeable energy storage technologies has become ever more pressing. Sodium-, potassium-, magnesium-, and zinc-ion batteries are fast becoming viable alternatives but are held back by capacity, rate and stability problems that have not developed comparably to lithium-ion batteries. To overcome these shortcomings and reduce the reliance on lithium, electrode materials used for these post-lithium batteries must be improved. Pre-intercalation of foreign species into the lattice of promising electrode materials can enhance their electrochemical performance in comparison to the un-pre-intercalated counterparts, closing the performance gap with lithium-ion batteries. This review article covers the common methods of pre-intercalating foreign species into electrode materials, the resulting structural effects and the improvements that are observed in the materials' electrochemical performance for post-lithium batteries. Timely and impactful work reported previously are summarised as examples of these improvements, demonstrating the value and ever-growing importance of pre-intercalation in today's battery landscape.

**Keywords:** Intercalation; Post-Lithium; Batteries; Energy Storage; Electrode Materials; Ion Diffusion; Active Sites

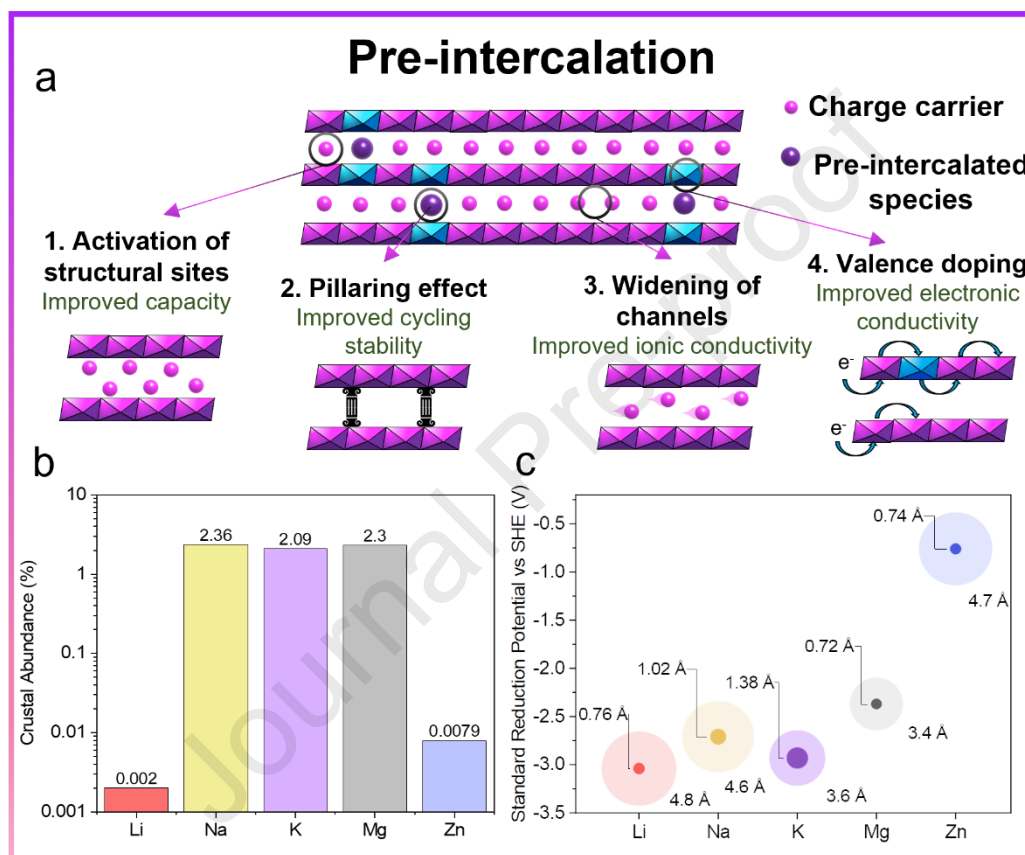
## 1. Introduction

Of the current energy storage technologies, lithium-ion batteries (LIBs) are among the most suited for tackling the current energy crisis and are one of the most important energy storage technologies of the 21st century [1]. They have permeated the lives of most people living in developed countries, being ubiquitous in handheld electronic devices, electric vehicles and home energy storage. However, the success of LIBs has also created a problem. The

production of lithium hydroxide, a precursor for many lithium electrodes, is very slow and can take up to 24 months from start to finish [2]. This creates a huge production bottleneck and results in rising prices, with lithium hydroxide costing £20,000 ton<sup>-1</sup> in Nov 2017 to now £69,000 ton<sup>-1</sup> in Nov 2022 [3]. Viable alternatives are needed. These come in the form of sodium-ion batteries (NIBs), potassium-ion batteries (KIBs), magnesium-ion batteries (MIBs) and zinc-ion batteries (ZIBs). Each of the alternatives to lithium (Li) have their own individual challenges and benefits when applied as charge carriers in batteries. To begin with, the most mature of these is sodium (Na) (Fig. 1b). The main benefits of Na<sup>+</sup> arise from its much higher crustal abundance, 2.3% vs 0.002%, and its smaller stokes radius, 4.6 Å vs 4.8 Å, than Li<sup>+</sup>. Crustal abundance is a reliable indicator of lower price, which is the largest factor in NIB's viability [4]. Na<sup>+</sup> also does not alloy with aluminum at low voltages, allowing for the more expensive and denser copper to be replaced as the anode current collector, raising the energy density of the battery and saving on material costs [5]. However, it does suffer from some downsides when compared to Li. Firstly, many common carbon anode materials require further modification to store Na<sup>+</sup> ions at any appreciable level. This is due to Na<sup>+</sup> poorly intercalating into graphite, forming NaC<sub>64</sub> and NaC<sub>186</sub>, which is very poor utilization when compared to LiC<sub>6</sub> or KC<sub>8</sub> [6, 7]. Secondly, while the stokes radius of Na<sup>+</sup> in propylene carbonate (PC) is smaller than Li<sup>+</sup>, its ionic radius is larger, 1.02 Å vs 0.76 Å [8]. Not only does this result in slower ion diffusion within the host lattice but also results in greater expansion and



contraction, promoting cracking and expulsion of the active material into the electrolyte, rendering it electrochemically inert. It is also more reactive than Li, making it difficult utilizing metal anodes on a commercial scale.



**Fig. 1.** (a) Schematic of pre-intercalation and its effects, along with the corresponding benefits for battery materials. (b) Crustal abundance of lithium, sodium, potassium, magnesium and zinc [9]. (c) Comparison of the  $M^+/M$  redox couple against the Standard Hydrogen Electrode (SHE), the Stokes and ionic radii of  $Li^+$ ,  $Na^+$ ,  $K^+$ ,  $Mg^{2+}$  and  $Zn^{2+}$ .

KIBs are another key alternative to LIBs. From their first reporting in 2004, KIBs have significantly advanced in terms of capacity, energy density, cycling stability and rate performance [10]. Potassium (K) has a similar crustal abundance to Na, making it a good fit for large scale applications where cost plays an even larger

factor. Its redox potential in propylene carbonate (PC) is even lower than  $\text{Li}^+$ , at  $-2.88$  V vs SHE. This could realize higher volumetric energy density cells than even LIBs, as the operating voltage is a key metric in energy density. In addition, the stokes radii of  $\text{K}^+$  in PC is even smaller than  $\text{Li}^+$  or  $\text{Na}^+$ ,  $3.6$  Å, indicating that KIBs could be a good candidate for fast charging and discharging [11]. However, this may be misleading, as KIBs suffer from problems associated with its larger ionic radius,  $1.43$  Å. This large size results in poorer ionic diffusion, greater expansion and contraction of the host lattice, lower energy density and lower specific capacity as fewer active sites have the space to accommodate it, compared to LIBs. It is also even more reactive to  $\text{H}_2\text{O}$  and  $\text{O}_2$  than Na, resulting in the obvious problems associated with having kilograms of highly reactive K in a highly mobile platform such as a vehicle, assuming a metal anode is used. Despite these drawbacks for mobile applications, both KIBs and NIBs show promise in the stationary energy storage sector and could be the key to realizing a fully renewable energy consuming society.

Moving away from alkali metals, ZIBs and MIBs are two other developing battery technologies. These ions benefit from being multivalent, as they can theoretically transport charge far more efficiently than monovalent ion. However, this benefit also appears as a problem, as because these ions are multivalent and they have a higher mass to charge ratios than  $\text{Li}^+$ , diffusion through electrolytes and materials are sluggish, due to larger hydration shells than  $\text{Na}^+$  or  $\text{K}^+$  (Fig. 1c) and stronger attraction/repulsion with the chemical environment within the host

lattice. Even with this problem, zinc in particular benefits from being able to utilize aqueous electrolytes, using water soluble zinc salts. This makes aqueous ZIBs far safer than alkali metal batteries, both because of the replacement of carbonate electrolyte and the reactivity of the metal anode [12]. Magnesium, in contrast, suffers mainly from electrolyte problems as the passivation layer formed on the surface of the magnesium hinders its stripping and plating, resulting in poor coulombic efficiency and rapid capacity decay [13]. As with Na and K, both magnesium and zinc are cheap and abundant, making them strong candidates for large scale energy storage.

When analysing the weaknesses of the LIB alternatives, some common themes start to emerge. In all cases, while the metals used are cheaper and/or more abundant than Li, the capacity or the stability of the electrode materials results in the practical energy density per  $\text{g}$  to be lower than LIBs, rendering them currently unviable. Their larger size or charge to size ratio vs  $\text{Li}^+$  also means that their diffusion in electrode hosts is more difficult, due to increased sterics and increased interactions with the surrounding atoms in the lattice. To become a practical alternative to LIBs, improvements to capacity, rate performance, stability, ionic and electronic conductivity are needed. This review highlights pre-intercalation as a valuable approach to tackle some of the problems faced by post-LIBs (Fig. 1a), by discussing the fundamental effects that are associated with pre-intercalation and the performance for NIBs, KIBs, ZIBs and MIBs.

Recent and impactful advances that have been made utilizing pre-intercalation are summarized and future perspectives are provided.

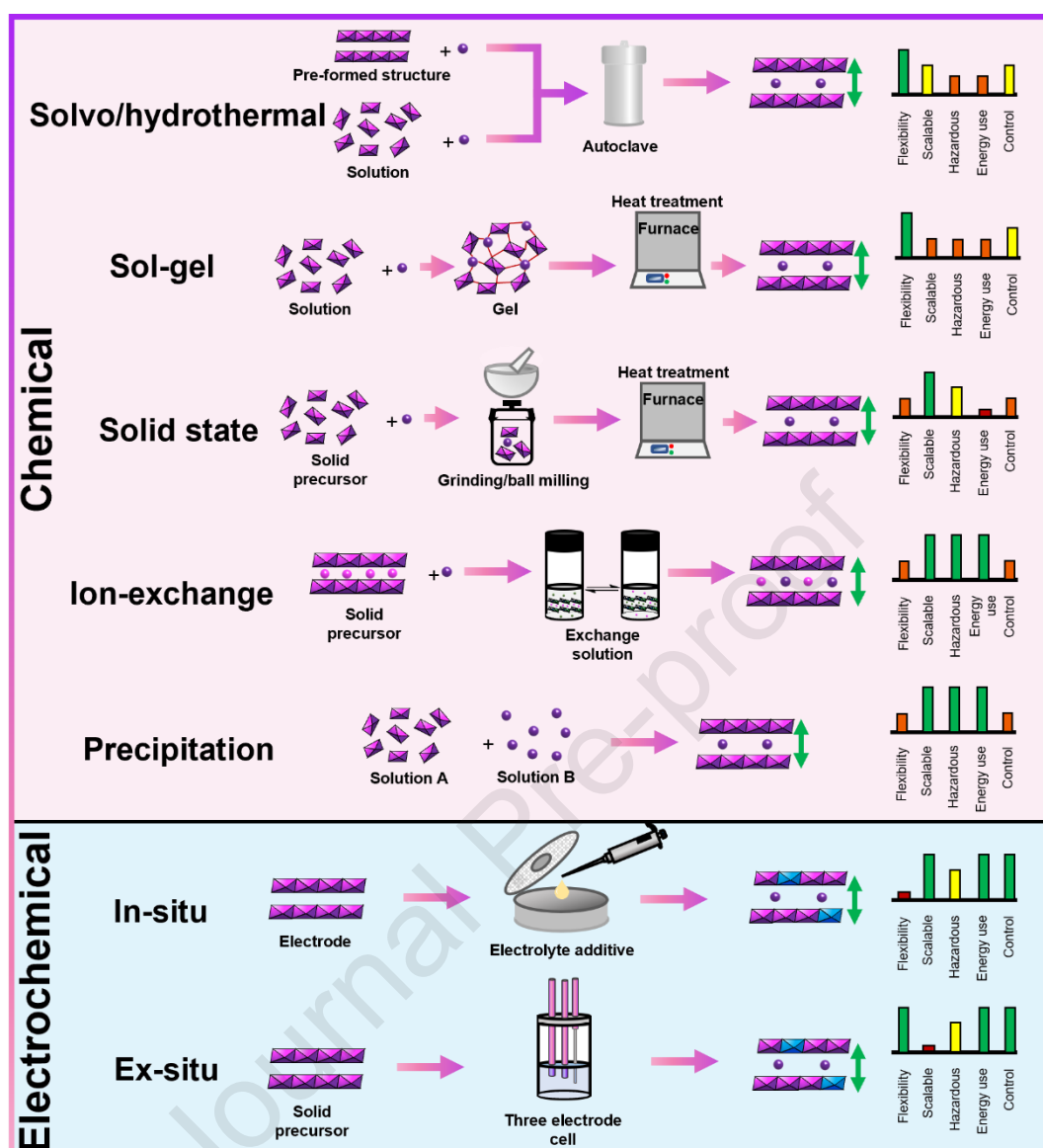
## **2. Pre-intercalation Background**

Since its first reporting in 1974, pre-intercalation has become an increasingly valuable approach to alter the properties of materials. This was followed by the pioneering work by Worrel in 1981, who investigated the pre-intercalation of alkali metal ions into  $\text{TiS}_2$  for LIBs [14]. In general, pre-intercalation involves the insertion of foreign ions or molecules into the host structure to assist the intercalation of further ions or molecules. Through a combination of steric and electronic effects, the pre-intercalated species modulates the structure-performance relationship of the material. Specifically for battery applications, pre-intercalation is primarily to alter the host structure to better accommodate the ions that are going to be cycled via the rocking chair mechanism, i.e., the charge carriers [15]. These alterations are performed to improve one or multiple of the problems associated with post-lithium-ion batteries, namely low capacity, poor performance at faster charge/discharge rates, and capacity loss on cycling.

### **2.1 Methods of Pre-intercalation**

There are two ways to pre-intercalate species into a host material, chemical and electrochemical pre-intercalation, each with their own benefits and drawbacks (Fig. 2). Chemical pre-intercalation commonly refers to the type of pre-intercalation performed during the synthesis of the material, such as during a

136 solvo/hydrothermal, sol-gel, precipitation, ion-exchange or solid-state reaction  
137 [16-19]. Out of these, solvo/hydrothermal is the most commonly used method  
138 due to its simplicity of use and the ability to form meta-stable phases under the  
139 high pressure and high temperature conditions, along with its industrial  
140 applicability. The pre-intercalated species may be added in the initial formation  
141 as a dopant or in a subsequent step, with the former providing greater control to  
142 the degree of pre-intercalation and the latter generally avoiding possible phase  
143 impurities.



**Fig. 2.** Summary of the common methods of pre-intercalation, along with a qualitative analysis of their relative performance in several areas of industrial relevance.

Sol-gel synthesis has gained significant popularity in recent years, due to its flexibility and low energy usage. However, a major hurdle is the reagents commonly used (e.g., titanium isopropoxide and niobium ethoxide), which are expensive and difficult to manufacture and handle, partially due to their propensity to react with moisture. This is currently limiting sol-gels industrial applicability. Ion-exchange, a large and distinct field of chemistry, has seen little

application in the battery industry, with no commercial materials utilising the process. This is understandable, as it has some significant hidden limitations. To perform ion-exchange, cations present in the material must be exchanged with cations in a surrounding media, which limits its use on cathodes, as any cations exchanged would likely not be de-intercalated upon charging, reducing the number of charge carriers and thus the capacity. Secondly, to perform ion-exchange, the material must already contain cations, thus ruling out many anode materials, such as carbonaceous materials and transition metal oxides (e.g., Ti and Nb oxides). Therefore, while ion-exchange is extremely attractive from a green chemistry point of view as it is often performed at room temperature and aqueous conditions, the pool of materials that can benefit from it are extremely limited [20]. In contrast, solid-state synthesis, is the most industrially relevant type of synthesis, as it is currently used in the manufacturing process of lithium cobalt oxide [21]. However, it suffers from poor energy use, often operating in excess of 800 °C, and is extremely limited in terms of morphology, secondary particle size, and pre-intercalation control. Finally, electrochemical pre-intercalation uses the driving force of the electric field generated by an applied voltage or current to insert species into the structure of the material [22, 23]. This can be done *ex-situ*, before cell assembly, or *in-situ*, using an additive to the electrolyte [24]. *Ex-situ* electrochemical pre-intercalation allows for maximum control over the pre-intercalation degree, but is difficult to perform and scale. *In-situ* pre-intercalation is significantly simpler, as the pre-intercalating species is

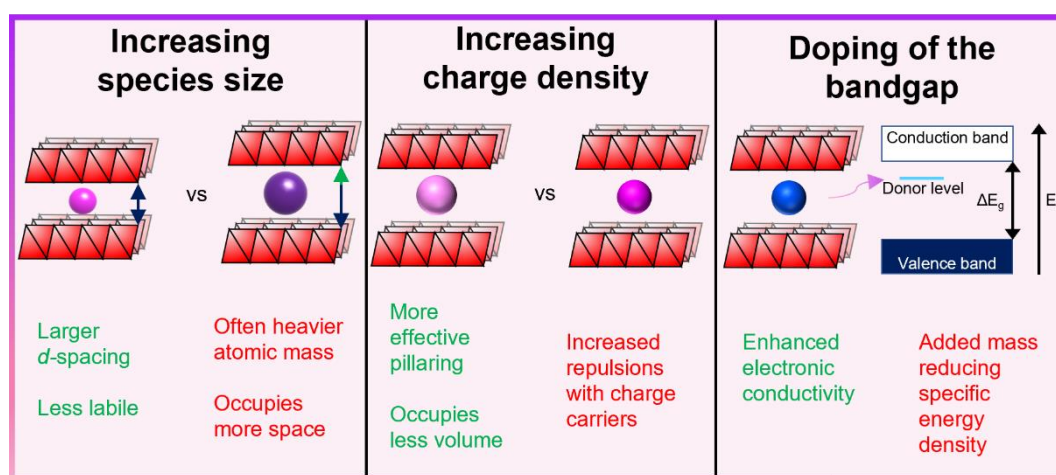
added directly to the electrolyte. However, this has much less control over the pre-intercalation degree than *ex-situ*, and the complication of additional species in the electrolyte can affect electrochemical stability and other unforeseen interactions, which potentially affects the SEI composition and growth.

Both the chemical and electrochemical approaches have different benefits and drawbacks, with the former being far more scalable and mature but having far less control over the degree of pre-intercalation than the latter [23]. However, electrochemical pre-intercalation provides access to synthetically challenging structures but results in greater structural damage to the electrode when compared to chemical pre-intercalation due to the lattice expansion, as its performed after fabrication of the electrode.

## 2.2 Pre-intercalated Species

Throughout the literature, there is a wide and diverse range of pre-intercalated species, which each has a unique effect on the particular structure type it is pre-intercalated into. There are several key attributes to pre-intercalated species, each with their own effects on the electrochemical attributes of the host lattice. The first attribute is the size of the species (left part of Fig. 3).



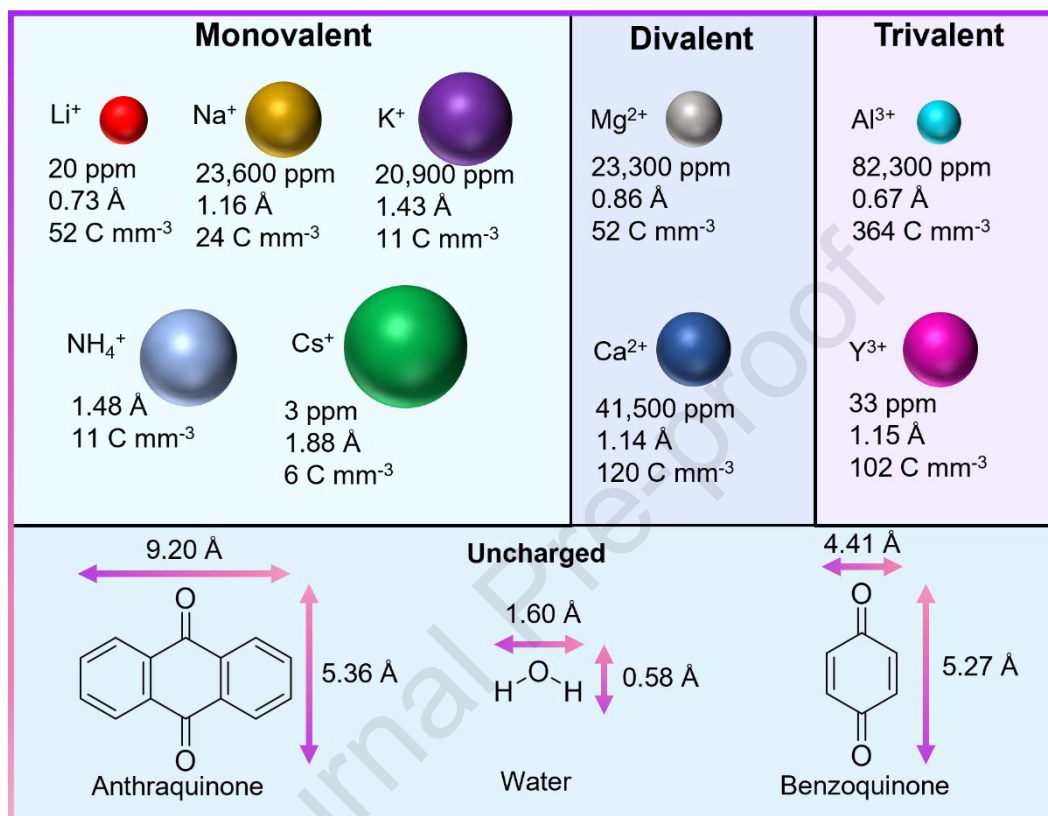


**Fig. 3.** Schematic displaying the effects of altering a pre-intercalating species size and charge density, along with doping effects.

With large species, for example  $K^+$ ,  $Rb^+$  and  $Cs^+$ , it has been well observed to increase the lattice spacing in layered structures, as they occupy larger volume with increasing atomic radius and have longer M–O bond lengths, directly increasing the *d*-spacing [25]. The increase in the *d*-spacing could help reducing cation–cation repulsion on charge and discharge, allowing for enhanced capacity and rate performance. However, intercalating large species consequentially takes up space that could otherwise be used for charge carriers, potentially resulting in a reduced capacity. This may also inactivate previously active sites, as the favourability of large species in relative to charge carriers may be preferred [26].

The second attribute is the charge density of the species (centre part of Fig. 3). These can range from the commonly found monovalent ions ( $Na^+$  and  $K^+$ ), to divalent ions ( $Mg^{2+}$  and  $Ca^{2+}$ ), trivalent ions ( $Al^{3+}$ ,  $Ti^{3+}$  and  $Fe^{3+}$ ) and charge-neutral species (anthraquinone and benzoquinone) [24, 27]. The species charge density and the associated hard–soft interactions with the host lattice polarise the local electronic environment to varying degrees, particularly for the higher

valence cations e.g.,  $\text{Fe}^{3+}$ ,  $\text{Ti}^{3+}$  and  $\text{Al}^{3+}$ , potentially resulting in enhanced electron affinity of the redox active cations (Fig. 4) [28].



**Fig. 4.** Representation of the species covered in this review, including size, charge density and crustal abundance (ppm) where applicable [9].

Furthermore, as the charge density of the pre-intercalated ions increases, the electrostatic repulsion with the charge carriers increases. This can have either positive or negative effects, depending on the level of pre-intercalation. With a low level (<0.1 per formula), the increased electrostatic interaction has been shown to be beneficial, with Sawangphruk *et al.* demonstrating that  $\text{Zn}^{2+}$  had a reduced binding energy to the lattice in pre-intercalated  $\delta\text{-MnO}_2$  when the species was the charge dense  $\text{Al}^{3+}$ , rather than  $\text{Ca}^{2+}$  or  $\text{Na}^+$  [29]. However, when the pre-

intercalation level is high, these electrostatic repulsions may result in more hindered diffusion and thus worsen rate performance [30].

The third attribute is the doping effect and orbital configuration of the pre-intercalated species (right part of Fig. 3). Species like alkali metals, which only have valence  $s$  orbitals, are not high enough in energy to mix with the  $d$  orbitals of transition metals, likely adding no extra levels in the bandgap of the host structure. However, they bring additional electrons into the host structure, acting as n-type dopants [31]. For example, through angle-resolved photoemission spectroscopy (ARPES), Takahashi *et al.* demonstrated that when  $\text{Ca}^{2+}$  was pre-intercalated into graphite, there were significant downfield shifts in the C  $2p$   $\pi$  and  $\sigma$  bands, resulting in significantly enhanced charge transfer kinetics [32]. In addition, through electrostatic and steric interactions they distort the surrounding lattice, and even slight deviations caused by the distortion can result in dramatic changes in the band structure, significantly improving conductivity relative to the non-pre-intercalated structure [33]. However, other transition metals like titanium and iron do have  $d$  orbitals available for such mixing, allowing for more traditional doping and additional levels within the band structure to improve electronic conductivity. Finally, the lability of the species must be considered carefully. In general, the greater the interaction of the pre-intercalated species with the surround host lattice, the higher the diffusion barriers are, and the less labile the species is. This aspect of pre-intercalation is significantly underdeveloped, but some general considerations can be made. While there are

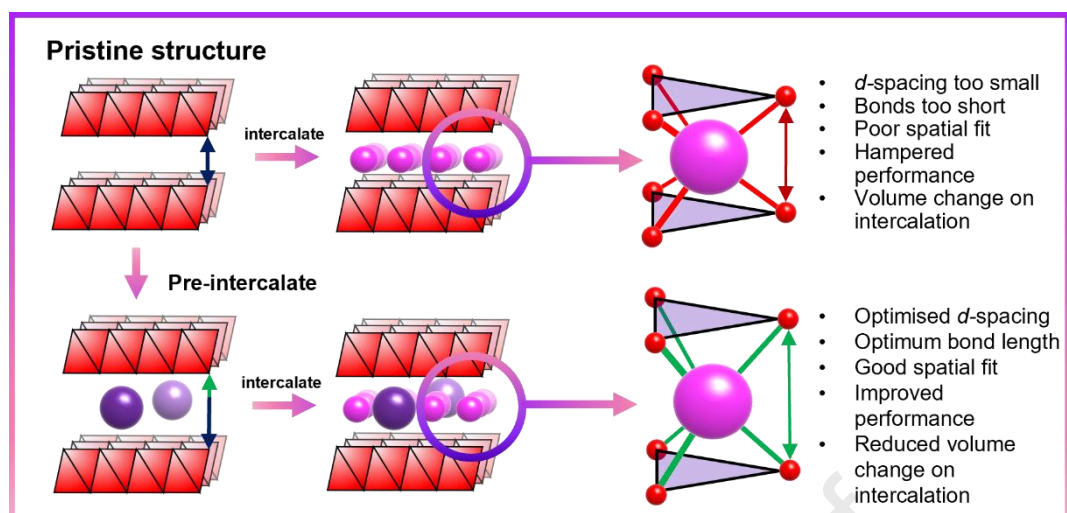
a multitude of factors that determine a species bonding strength, it can be roughly judged via the predicted bond length between the atoms in the host lattice and the pre-intercalated species, as bond length is a reasonable proxy for bond strength [34]. In many cases, it is a metal–oxygen bond that is formed, as many of the examples are metal cations intercalating into oxygen containing lattices. The stronger the metal–oxygen bond is, the less the likelihood of the species is to be highly labile than the charge carrier is [25]. In addition, the larger the cation is, the more oxygens it is able to interact with, further reducing its lability, which is the root cause of many problems with KIBs and NIBs. However, in-depth research is required in this aspect of pre-intercalation, as very little conclusive evidence has been produced on the lability and effects of the de-intercalation of these species after long term cycling.

### **2.3 Pre-intercalated Hosts**

As vital as pre-intercalated species, the crystal and electronic structures of the host lattice must be analysed carefully when pre-intercalation is considered. With the vast number of crystal structures under investigation in the energy storage literature, a comprehensive coverage would be near futile, but general themes can undoubtedly be gleamed. The crystal structures can be generally categorised into two types, layered and tunnelled.

Layered materials, in this context, are comprised of two-dimensional (2D) sheets with space in between the sheets for charge carriers to intercalate into. These 2D

interlayer spaces allow intercalating ions to diffuse in a plane, speeding up diffusion through the structure and reducing overpotential, despite some slight preferential diffusion directions that have been observed in some materials [35]. The stacking arrangement of these sheets gives rise to the three most common layered intercalation based active materials with the formula  $A_yMX_2$  ( $0 \leq y \leq 1$ ), which are O1, O3 and P3 respectively [36]. These are so named for the octahedral and prismatic sites that they contain, with significant differences in ion selectivity between them. As the octahedral sites are larger, forming longer M–X bond lengths with the intercalating charge carriers, these preferentially intercalate larger cations, such as  $Na^+$  and  $K^+$  that are more able to fill the site and stabilise the structure [36]. While the P-type structures can still intercalate the larger ions, they are less favoured, resulting in reduced capacity. This expands upon the structure–performance relationship of the material, as by modulating the interlayer spacing via pre-intercalation, the volume of these sites can be altered, improving their selectivity towards larger ions, thus improving their performance (Fig. 5).



**Fig. 5.** Schematic displaying the effect of optimized  $d$ -spacing on the local environment of the charge carriers, resulting in enhanced electrochemical performance.

This logic extends to other layered materials such as  $\alpha$ - $\text{V}_2\text{O}_5$  or  $\text{Na}_2\text{Ti}_3\text{O}_7$ . For tunnelled-type structures, the structure–performance relationship between the pre-intercalated species and host lattice is much harder to predict. The size of the channel is a significant limiting factor here, as pre-intercalating a species with greater interactions with the lattice than the charge carriers may block channels, effectively making the channel unusable for ion diffusion. However, it has been demonstrated that large channels such as those in  $\alpha$ - $\text{MnO}_2$ , can benefit pre-intercalation, as the ability of the pre-intercalated species to block channels is offset by the absolute size of the channel vs the size of the charge carriers [37].

The difference in applicability can be inferred from the most common structures for pre-intercalation, which are overwhelmingly layered type materials. There is a significant research deficiency in pre-intercalating tunnelled type structures, particularly spinel and NASICON structures. In one of the rare examples, Masquelier *et al.* described the electrochemical pre-intercalation of  $\text{Na}^+$  into  $\text{Na}_3\text{FeV}(\text{PO}_4)_3$  NASICON-type structure, but concluded that while initial cycles

were improved, the valence change of  $\text{Fe}^{3+}$  to  $\text{Fe}^{2+}$  to accommodate the pre-intercalation resulted in significant capacity fading, as the reduction back to  $\text{Fe}^{2+}$  was kinetically slow [22, 23]. Further studies into tunnelled structures would be valuable additions to the pre-intercalation literature. While there is clearly significant nuance and variation within these two groupings, most common materials can be assigned to these two.

**Table 1:** Summary of pre-intercalated hosts covered, along with the pre-intercalated ions and their effects.

Species	Material	Method	Structure type	Ion-battery	$\Delta d$ (nm)	Stabilised performance	Ref
$\text{K}^+/\text{Na}^+$	C	Molten Salt	Soft Carbon	KIB	+0.018	325 mAh $\text{g}^{-1}$ @ 100 mA $\text{g}^{-1}$	[44]
$\text{K}^+$	C	HEBM	Soft Carbon	KIB	—	302 mAh $\text{g}^{-1}$ @ 50 mA $\text{g}^{-1}$	[46]
$\text{Na}^+$	$\delta\text{-Na}_{0.36}\text{V}_2\text{O}_5$	Hydrothermal	Layered	NIB	+0.690	179 mAh $\text{g}^{-1}$ @ 20 mA $\text{g}^{-1}$	[50]
$\text{K}^+$	$\delta\text{-K}_{0.42}\text{V}_2\text{O}_5 \cdot n\text{H}_2\text{O}$	Hydrothermal	Layered	KIB	-0.185	167 mAh $\text{g}^{-1}$ @ 20 mA $\text{g}^{-1}$	[53]
$\text{K}^+$	$\text{K}_{0.22}\text{V}_{1.74}\text{O}_{4.37} \cdot 0.82 \text{H}_2\text{O}$	Precipitation	Layered	KIB	+0.350	183 mAh $\text{g}^{-1}$ @ 5 mV $\text{s}^{-1}$	[54]
$\text{Na}^+$	$\text{Na}_{0.71}\text{K}_{0.29}\text{MnO}_2$	Hydrothermal	Layered	NIB	-0.04	130 mAh $\text{g}^{-1}$ @ 1.5C	[41]
$\text{K}^+$	$\delta\text{-K}_{0.42}\text{MnO}_2$	Precipitation	Layered	ZIB	increase	130 mAh $\text{g}^{-1}$ @ 300 mA $\text{g}^{-1}$	[55]
$\text{K}^+/\text{Na}^+/\text{Li}^+$	$\text{M}_{0.7}\text{Fe}_{0.5}\text{Mn}_{0.5}\text{O}_2$	Precipitation	Layered	NIB	+0.221	181 mAh $\text{g}^{-1}$ @ 100 mA $\text{g}^{-1}$	[56]
$\text{K}^+$	$\text{K}_{0.25}\text{TiS}_2$	Chemical Treatment	Layered	KIB	+0.193	135 mAh $\text{g}^{-1}$ @ 24 mA $\text{g}^{-1}$	[60]
$\text{NH}_4^+/\text{K}^+$	$\text{K}_{0.5}\text{V}_2\text{O}_5$	Hydrothermal	Layered	KIB	+0.501	71 mAh $\text{g}^{-1}$ @ 25 mA $\text{g}^{-1}$	[62]
$\text{H}_2\text{O}$	$\text{V}_2\text{O}_5 \cdot 0.6\text{H}_2\text{O}$	Hydrothermal	Layered	KIB	+0.888	103 mAh $\text{g}^{-1}$ @ 50 mA $\text{g}^{-1}$	[63]
$\text{Y}^{3+}$	$\text{Y}_{0.06}\text{V}_2\text{O}_5$	Sol-gel	Layered	NIB	+0.25	119 mAh $\text{g}^{-1}$ @ 100 mA $\text{g}^{-1}$	[30]
$\text{Al}^{3+}$	$\text{H}_{11}\text{Al}_2\text{V}_6\text{O}_{23.2}$	Hydrothermal	Layered	ZIB	+0.886	260 mAh $\text{g}^{-1}$ @ 1 A $\text{g}^{-1}$	[64]
$\text{Al}^{3+}$	$\alpha\text{-MnO}_2$	Hydrothermal	Tunnelled	ZIB	+0.05	401 mAh $\text{g}^{-1}$ @ 100 mA $\text{g}^{-1}$	[37]
$\text{Al}^{3+}$ , anthraquinone	$\text{V}_2\text{O}_5$	Hydrothermal	Layered	ZIB	+0.95	400 mAh $\text{g}^{-1}$ @ 1 A $\text{g}^{-1}$	[24]
$\text{Al}^{3+}$ , benzoquinone	$\text{V}_2\text{O}_5$	Hydrothermal	Layered	ZIB	+0.024	332 mAh $\text{g}^{-1}$ @ 1 A $\text{g}^{-1}$	[27]
$\text{K}^+$	$\text{Ti}_3\text{C}_2\text{T}_x\text{-MXene}$	Chemical Treatment	Layered	KIB	+0.02	70 mAh $\text{g}^{-1}$ @ 1 A $\text{g}^{-1}$	[71]
$\text{Ca}^{2+}$	$\text{CaV}_8\text{O}_{20} \cdot 3\text{H}_2\text{O}$	Hydrothermal	Layered	NIB	+0.628	252 mAh $\text{g}^{-1}$ @ 200 mA $\text{g}^{-1}$	[61]
$\text{K}^+$	$\text{TiS}_2$	Electrochemical	Layered	NIB	+0.122	124 mAh $\text{g}^{-1}$ @ 5C	[73]
$\text{Cs}^+/\text{Na}^+$	$\text{Na}_{0.33}\text{Cs}_{0.03}\text{V}_2\text{O}_5$	Hydrothermal	Tunnelled	ZIB	+0.014	313 mAh $\text{g}^{-1}$ @ 200 mA $\text{g}^{-1}$	[74]
$\text{Mg}^{2+}/\text{H}_2\text{O}$	$\text{Mg}_{0.5}\text{V}_2\text{O}_5 \cdot 1.1\text{H}_2\text{O}$	Hydrothermal	Layered	MIB	+0.12	164 mAh $\text{g}^{-1}$ @ 100 mA $\text{g}^{-1}$	[75]
$\text{Na}^+$	$\text{NaMnO}_{2-y}\delta(\text{OH})_{2y}$	Hydrothermal	Layered	NIB	+0.18	137 mAh $\text{g}^{-1}$ @ 10C	[82]
$\text{K}^+$	$\text{K}_{0.20}\text{VS}_4$	Electrochemical	Layered	MIB	increase	194 mAh $\text{g}^{-1}$ @ 50 mA $\text{g}^{-1}$	[83]
$\text{Na}^+$	$\text{Na}_{0.33}\text{V}_2\text{O}_5$	Hydrothermal	Layered	ZIB	+0.374	341 mAh $\text{g}^{-1}$ @ 100 mA $\text{g}^{-1}$	[84]
$\text{Na}^+$	$\text{Na}_3\text{FeV}(\text{PO}_4)_3$	Electrochemical	Tunnelled	NIB	increase	110 mAh $\text{g}^{-1}$ @ C/20	[23]



### **3. Effects of Pre-Intercalation**

#### **3.1 Activating Structural Sites**

Within the crystal structure of every intercalation-based active material, there are active sites that can favourably accommodate the charge carrier ions. For example, in O3 and P3 type layered metal oxides, these sites are the octahedral and prismatic sites between the layers, respectively. By engineering the interlayer spacing via pre-intercalation, the spatial volume of these sites can be increased or decreased, optimising the site for improved interactions between the intercalating charge carrier and the lattice. This concept is well applied in other areas of research such as coordination chemistry, but is rarely applied in the energy storage field [26]. As the size of the intercalating ion may be too large, some sites may not be readily accessible or optimised for occupation, thus by understanding this optimisation of spatial fit, the possible sites in a material may be activated through enlarging or reducing their volume, thus improving capacity.

In addition, common methods such as enhancing conductivity through carbon coating or advanced electrolyte formulations will have no effect on the inherent crystal structure of the material, thus providing no assistance to the activation or optimisation of such active sites. Thus, pre-intercalation is ideally suited to improve these inactive sites, as by pre-intercalating larger pillaring ions or molecules, lattice spacing can be expanded, allowing for greater access to favourable sites for charge storage [38, 39]. While this does occur during charge



and discharge, often the degree of volume change is very limited, <25%, whereas pre-intercalation can produce dramatic *d*-spacing changes, up to 100% increases [40, 41]. This can provide access to more active sites than is achieved through the charge–discharge expansion and contraction. For active sites that are oversized for the corresponding ion, interactions with the surrounding lattice can improve the spatial fit of subsequent intercalating ions. By increasing the distance between the layers of a material, the greater volume of free space there is to store intercalating charge carriers, so an improvement to the specific capacity of the pre-intercalated material is anticipated. This activation effect is also more commonly seen in battery types that use cations with a larger radius, such as Na<sup>+</sup> and K<sup>+</sup>, as these cations are the most affected by the size of active sites [42]. Smaller ions such as Li<sup>+</sup>, Zn<sup>2+</sup> and Mg<sup>2+</sup>, are less sterically hindered by the surrounding lattice, so pre-intercalation may not improve capacity to a great extent, as there already exists adequate access to most of the active sites. This is displayed in the number of recent reviews that display a focus on utilising pre-intercalation to improve the specific capacity of a material, which are primarily Na and K-based batteries [42, 43]. Due to the facile nature of pre-intercalation, it can be applied to a wide variety of materials. Liu et al. utilised pre-intercalation via a molten salt, a KCl/NaCl mix with a 1:1 molar ratio, which was added to a mix of soft carbon, sulphur powder and urea to produce K<sup>+</sup> intercalated nitrogen and sulphur doped soft carbon (NSC) nanosheets for use as an anode in KIBs [44]. The K content was estimated to be 1.23 at.%, by energy-

dispersive X-ray spectroscopy (EDS). As pre-intercalation content is an important variable, further determination of K content via inductively coupled plasma optical emission spectroscopy (ICP-OES) and X-ray photoelectron spectroscopy (XPS), would be beneficial to fully emphasise the effect of pre-intercalated K on performance. Transmission electron microscopy (TEM) results revealed an interlayer distance of 0.378 nm, which was corroborated by X-ray diffraction (XRD), whereas comparative literature values for non-potassiated NSCs have been reported as 0.36 nm, a clear increase that can be clearly ascribed to the pre-intercalated  $K^+$  [45]. This increase was then demonstrated to increase the capacity, as the pre-potassiated NSC averaged  $325 \text{ mAh g}^{-1}$  compared to an average of  $220 \text{ mAh g}^{-1}$  for the non-pre-intercalated NSC, at the same rate of  $100 \text{ mA g}^{-1}$  over the first 10 cycles. Through density-functional theory (DFT) calculations, the synergistic effect of  $K^+$  pre-intercalation and heteroatom doping were investigated, indicating that a combination of improved K-adsorption energies, enlarged interlayer spacing and reduced migration barriers were the reasons for the enhanced capacity and kinetics observed.

Further investigating carbon materials, pre-potassiated amorphized carbon black (K-aCB) was investigated by Park *et al.* via high-energy ballmilling (HEM) with metallic K, followed by the  $500^\circ\text{C}$  annealing as an anode for KIBs [46]. The level of pre-potassiation was only confirmed via electron energy loss spectroscopy (EELS) and EDS. The interlayer spacing was observed to be expanded. For performance, the K-aCB achieved a reversible capacity of

mAh g<sup>-1</sup> over 200 cycles, as well as 337 mAh g<sup>-1</sup> on the first discharge and 407 mAh g<sup>-1</sup> on the first charge, corresponding to a 120.7% initial coulombic efficiency. The aCB and CB showed a reversible capacity of 175 mAh g<sup>-1</sup> and 74 mAh g<sup>-1</sup>, respectively. With the amorphization control showing much lower capacity, the increase in performance was ascribed to the pre-potassiation reducing irreversible reactions common in the first cycle. However, due to the partially amorphous nature of the carbon, any graphitic regions remaining would have been expanded due to the pre-intercalation of K<sup>+</sup>, allowing for greater access to those sites, thus further increasing the capacity.

Utilizing pre-intercalation to boost access to active sites is not only limited to carbonaceous materials, with layered vanadium oxides being a common subject of pre-intercalation investigation. Vanadium oxides have been the subject of intensive research for decades. Since the first successful demonstration in NIBs in 2011, many avenues have been explored to improve the performance in line with LIB benchmarks, such as phase optimization, nanostructural control, doping and carbon coating [47-49]. Even with the success of these methods, pre-intercalation stands out as a major factor in the improvement of vanadium oxides as a cathode material for NIBs and KIBs. Pomerantseva *et al.*, utilising previous work for LIBs, reported a chemically pre-intercalated  $\delta$ -V<sub>2</sub>O<sub>5</sub> as a cathode for NIBs [50]. By optimising the aging times for the chemical pre-intercalation to occur, a maximum ratio of Na:V of 0.36 was observed in a pure bilayered  $\delta$ -Na<sub>x</sub>V<sub>2</sub>O<sub>5</sub> phase, with a large interlayer spacing of 11.4 Å. This phase

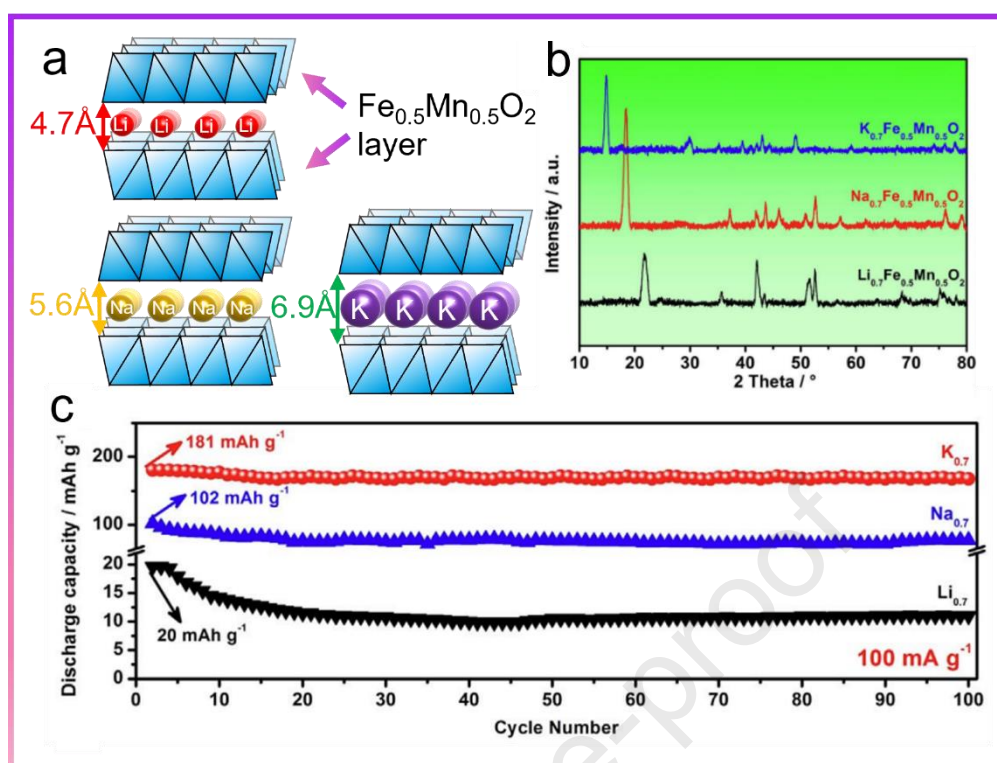
rearrangement, from orthorhombic  $\alpha$ -V<sub>2</sub>O<sub>5</sub> to  $\delta$ -Na<sub>x</sub>V<sub>2</sub>O<sub>5</sub>, along with the corresponding interlayer spacing increase, from 4.5 Å to 11.4 Å, provided far greater access to the redox active sites for the intercalating Na<sup>+</sup> ions, which was reflected in the capacity. The optimised  $\delta$ -Na<sub>x</sub>V<sub>2</sub>O<sub>5</sub> achieved a 365 mAh g<sup>-1</sup> first discharge and a ~320 mAh g<sup>-1</sup> 2<sup>nd</sup> charge, significantly larger than previous capacities for vanadium oxides [47, 51, 52]. However, this capacity was poorly retained, with it dropping to 179 mAh g<sup>-1</sup> after 30 cycles, with no longer term cycling characterisation performed, indicating that possibly the performance continued to decrease on cycling. Pomerantseva *et al.* went on to repeat this work for KIBs, demonstrating a potassiation of  $\delta$ -K<sub>0.42</sub>V<sub>2</sub>O<sub>5</sub>·nH<sub>2</sub>O, with an interlayer distance of 9.65 Å [53]. This is a reduction from pristine  $\delta$ -V<sub>2</sub>O<sub>5</sub>, at 11.5 Å, which was ascribed to a lower water content, with only 1 row of water molecules in the interlayer spacing, rather than the usual 2 for other alkali metals. This is an example of interlayer optimisation, as interactions with the pre-intercalated species reduced the interlayer spacing, improving interactions for subsequently intercalated species. This  $\delta$ -K<sub>0.42</sub>V<sub>2</sub>O<sub>5</sub>·nH<sub>2</sub>O displayed a 1<sup>st</sup> discharge of 268 mAh g<sup>-1</sup> with good stability, retaining 74% when cycling at 20 mA g<sup>-1</sup>. Analysing the structure–performance relationship demonstrates that reduction in interlayer spacing can also improve performance, indicating that interlayer spacing optimisation is more important to improvements in capacity, rather than absolute size. In general, if the interlayer spacing is initially small, pre-intercalation of larger species can expand the structure and provide more volume

for the charge carriers to occupy sites, thus activating them, while weakening coulombic interactions with the negatively charged layers. If the  $d$ -spacing is already very large, pre-intercalated species can contract the layers, shortening the distance between the layers and stabilising the charge carriers.

Teng *et al.* demonstrated the improvement that pre-intercalated interlayer water can have on amorphous materials in aqueous KIBs, with the disordered  $\text{K}_{0.22}\text{V}_{1.74}\text{O}_{4.37} \cdot 0.82 \text{H}_2\text{O}$  out performing commercial  $\text{V}_2\text{O}_5$ , achieving  $183 \text{ mAh g}^{-1}$  and  $\sim 43 \text{ mAh g}^{-1}$  respectively [54]. This was ascribed to the pre-intercalated water molecules interacting with the  $[\text{VO}_6]$  octahedra and inducing local structural rearrangements, along with structural distortions caused by the  $\text{K}^+$  ions. A synergistic effect between the pre-intercalated water and  $\text{K}^+$  was posited, that the disordered structure allowed for a wider potential window for  $\text{K}^+$  intercalation, improving storage. However, it is possible that the local deformations caused by the pre-intercalated  $\text{K}^+$ , further stabilised by the water molecules, also contributed to the increase in capacity.

Manganese oxide materials have also been demonstrated to show improvements to capacity with pre-intercalation, with Shao *et al.* utilising pre-intercalation to improve the capacity of Birnessite-type ( $\text{A}_x\text{MnO}_{2+y}$ ) materials in NIBs [41]. Commonly, only one metal cation is intercalated into Birnessite-type manganese oxides, but for this work, both  $\text{Na}^+$  and  $\text{K}^+$  were pre-intercalated. This has the synergistic effect of reducing the amount of cations lost via irreversible processes, as well as utilising the  $\text{K}^+$  ions to provide adequate access to the active

sites. The 15:1 Na:K sample showed an improved discharge capacity of  $\sim 130$  mAh  $\text{g}^{-1}$  when compared to the  $\text{KMnO}_2$  that achieved  $\sim 80$  mAh  $\text{g}^{-1}$ . However, this effect was lost when the ratio of  $\text{K}^+$  in the synthesis was reduced above 22.5:1 Na:K. This smaller interplanar spacing would reduce the availability of active sites for the  $\text{Na}^+$  ions, which had previously been kept available by the  $\text{K}^+$  ions, which would explain the decrease in performance. This effect was also observed by Yu et al. using alkali ion pre-intercalated  $\delta\text{-MnO}_2$  in ZIBs, as the  $\text{K}_{0.42}\text{MnO}_2$  out-performed the  $\text{Na}_{0.43}\text{MnO}_2$  and  $\text{Li}_{0.52}\text{MnO}_2$ , in capacity, rate performance and cycling stability and was attributed to the greater structural integrity the larger  $\text{K}^+$  provided [55]. The structure-performance relationship between the host and the pre-intercalated species can be clearly indicated via the larger  $\text{K}^+$  ions expanding the interlayer spacing, increasing the volume of the active sites and improving the capacity, despite also taking up more volume concurrently. The lower charge density of the  $\text{K}^+$  also results in less electrostatic repulsion, thus enabling to store more  $\text{Zn}^{2+}$  in the available volume.



**Fig. 6.** (a) Schematic displaying the effects of varying the size of the pre-intercalated alkali ion on the  $d$ -spacing of crystal structure. (b) XRD patterns of iron manganese oxides pre-intercalated with various alkali metal ions, from  $\text{K}^+$  to  $\text{Li}^+$ . (c) cycling performance of the pre-intercalated iron manganese oxides, at 100  $\text{mA g}^{-1}$ . Reproduced with permission from Ref. [56]. Copyright © 2017 Elsevier Ltd.

Mai *et al.* reported a  $\text{K}^+$  ion pre-intercalated iron-manganese oxide,  $\text{K}_{0.7}\text{Fe}_{0.5}\text{Mn}_{0.5}\text{O}_2$  for NIBs [56]. They investigated the electrochemical performance of  $\text{K}_{0.7}\text{Fe}_{0.5}\text{Mn}_{0.5}\text{O}_2$ ,  $\text{Na}_{0.7}\text{Fe}_{0.5}\text{Mn}_{0.5}\text{O}_2$  and  $\text{Li}_{0.7}\text{Fe}_{0.5}\text{Mn}_{0.5}\text{O}_2$  (Figs. 6a and b) with each sample also being carbon coated. There was a stark difference between samples, with the  $\text{Li}^+$  pre-intercalated sample producing 20  $\text{mAh g}^{-1}$  of capacity on discharge at 100  $\text{mA g}^{-1}$ , in comparison to the  $\text{Na}^+$  and  $\text{K}^+$  containing samples, that achieved 102 and 181  $\text{mAh g}^{-1}$  respectively, at the same current density (Fig. 6c). Over 100 cycles this capacity was retained by 93%, 76% and 56% for the K, Na and Li containing material respectively. The K-containing

version also exhibited the highest interlayer spacing, at 6.94 Å, and the lowest  $R_{ct}$  of the tested samples. This again reinforces both the structure-performance relationship and the host-guest relationship, as widening the  $d$ -spacing results in the increased volume of the active sites and thus increased capacity, despite larger  $K^+$  occupying more space than  $Na^+$  or  $Li^+$ .

Pre-intercalation has been demonstrated to be an effective way to improve the capacity of electrode materials in NIBs, KIBs and aqueous KIBs. The primary mechanism by which pre-intercalation was observed to improved capacity was generally through the expansion of the interlayer spacing. This allows for more species to be incorporated into the structure, as the electrostatic repulsion between the charge carriers could be reduced with increasing distance between them. Exceptions to this rule were covered but were limited to vanadium materials with exceptionally large  $d$ -spacings [54]. The type of species appears to be an essential factor, as the species needs to be large enough to adequately expand the interlayer spacing to optimise for further ion intercalation. However, pre-intercalating too many species can have detrimental effects, as the larger pre-intercalated species can block active sites if in excess, as seen with  $KMnO_2$ , so optimisation is required. The primary beneficiaries of this effect are layered-type materials, as  $Na^+$  and  $K^+$  can struggle to diffuse into the layers if they are not sufficiently widened.

### 3.2 Pillaring to Reduce Lattice Expansion and Contraction



The pillaring effect of pre-intercalated species in layered structures is one of the most beneficial and most studied effects of pre-intercalation [57]. The pre-intercalating species fills the sites between the layers, holding the layers at a more optimum distance for further ion intercalation, reducing expansion and contraction of the lattice, which consequently minimises pulverisation of the electrode and improves stability. Although this reduces the volumetric energy density slightly, the improvement to the stability often outweighs the reduction of volumetric energy density. The pillaring effect can expand or contract the interlayer spacing, as discussed previously, as the  $d$ -spacing can decrease if the intercalated species is positive, shielding the two negative layers more effectively from each other. This pre-intercalation effect is vitally important in the post-LIB types, as poor cycling stability is an almost ubiquitous problem, as the larger sizes or larger charges of the cations vs  $\text{Li}^+$  induce larger volume changes on intercalation and deintercalation. Metal sulphides, in particular  $\text{TiS}_2$ , were some of the first materials examined for use in LIBs, but have struggled to gain traction commercially [58, 59]. This is because despite high capacity,  $\text{TiS}_2$  is marred by complex phase transitions, disproportionation reactions and sulphide shuttling, which rapidly degrade battery performance on cycling [60]. Loh *et al.* investigated  $\text{TiS}_2$  as a cathode for KIBs by pre-potassiating it to form  $\text{K}_{0.25}\text{TiS}_2$  (Fig. 7a) [60]. This was demonstrated to have improved cycling performance than bulk  $\text{TiS}_2$ , retaining  $\sim 135 \text{ mAh g}^{-1}$  after 120 cycles at  $24 \text{ mA g}^{-1}$ , compared to  $\sim 80 \text{ mAh g}^{-1}$  from the  $\text{TiS}_2$ . This was investigated via *in-situ* XRD, with an

unstable buffer phase observed when K content is between 0.1 and 0.25. This buffer phase ( $2^k$ ) is irreversible upon charging, being unable to be charged back to  $\text{TiS}_2$  and resulting in significant  $\text{K}^+$  loss upon formation. By forming a phase with a higher K content of 0.25 per formula chemically, the associated structural deformation from pristine  $\text{TiS}_2$  to the buffer phase is bypassed and much less  $\text{K}^+$  is removed from the system, demonstrated by a lower irreversible initial discharge capacity and a higher ICE (Figs. 7b and c). This phenomenon is likely to occur in many other material, as irreversible phase transformations are very common sources of initial capacity loss, but is rarely investigated in depth, indicating a fruitful area of further research [61]. Vanadium oxides, while concretely demonstrated to show higher capacity capability with pre-intercalation, also show improved stability by pillaring the pre-intercalated ions between the layers. The relationship between the size of interlayer spacing and the performance has already been analysed, with a clear trend that optimisation is better than absolute distance, but this had yet to be demonstrated from a stability perspective. To investigate the pillaring effect on the stability of vanadium oxides, Zhang *et al.* compared the stability of several pre-intercalated vanadium oxides,  $\text{NH}_4\text{V}_3\text{O}_8$ ,  $(\text{NH}_4)_{0.5}\text{V}_2\text{O}_5$  and  $\text{K}_{0.5}\text{V}_2\text{O}_5$  for KIB cathodes [62].

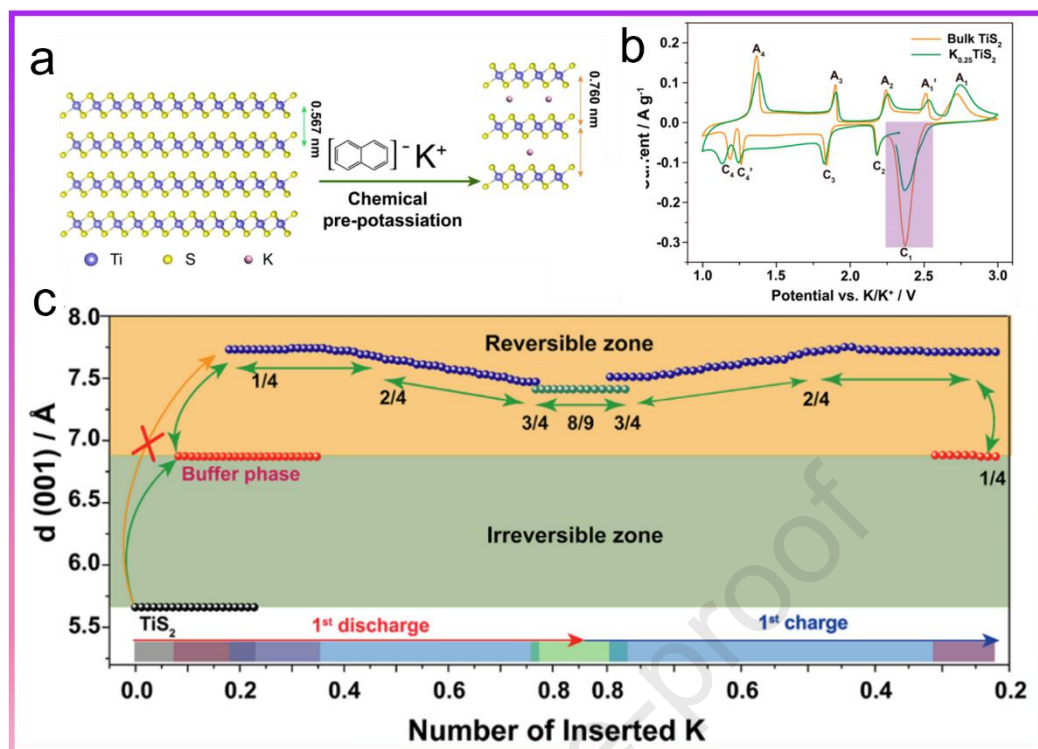


Fig. 7. (a) Schematic displaying the pre-intercalation of  $\text{K}^+$  into the  $\text{TiS}_2$  layers. (b) CV curves of  $\text{TiS}_2$  and  $\text{K}_{0.25}\text{TiS}_2$  demonstrating a skipping of  $\text{C}_1$  on first discharge. (c) Schematic displaying the SOC versus the  $d$ -spacing of the (001) reflection, with irreversible phases indicated. Reproduced with permission from Ref. [60]. Copyright © 2017, American Chemical Society.

These were observed to have an interlayer spacing of 7.78 Å, 9.56 Å and 9.37 Å respectively, compared to 4.36 Å for the  $\text{V}_2\text{O}_5$  control. Despite the presence of hydrogen bonding between the  $\text{NH}_4^+$  and V-O layers, the stability of both  $\text{NH}_4\text{V}_3\text{O}_8$  and  $(\text{NH}_4)_{0.5}\text{V}_2\text{O}_5$  was far worse than the  $\text{K}^+$  pre-intercalated  $\text{K}_{0.5}\text{V}_2\text{O}_5$ , as they achieved a capacity retention of 20.2 and 59.1% respectively, to the 83.5% the  $\text{K}_{0.5}\text{V}_2\text{O}_5$  achieved. This result was attributed to layer collapse and irreversible structural destruction caused by the de-intercalation of the larger  $\text{NH}_4^+$ . This is a clear example of one of the major problems pre-intercalation faces, the retention of the pillaring species. If the pillaring species is too labile, it

can de-intercalate on cycling, causing both the pillaring effect to be reduced and because it is often larger than the charge carrier ions, it causes more structural damage than the charge carriers, leading to worse cycling stability. This is a particular problem with water intercalated materials, as during cycling the crystalline water can be de-intercalated into the electrolyte and undergo electrolysis, which forms species that catalyse electrolyte breakdown and severely reduce battery performance. This was observed for  $\text{V}_2\text{O}_5 \cdot 0.6 \text{H}_2\text{O}$  in KIBs by Li *et al.*, that used pre-intercalated water to stabilise the interlayer space of the  $\text{V}_2\text{O}_5$  sheets [63]. The discharge capacity dropped from  $225 \text{ mAh g}^{-1}$  to  $\sim 100 \text{ mAh g}^{-1}$  over 50 cycles, only to rise back up to  $\sim 175 \text{ mAh g}^{-1}$  by 250 cycles. This inconsistent capacity was attributed to the water de-intercalating, increasing side reactions and possibly forming KOH, but also making space for further  $\text{K}^+$  intercalation. One strategy to stabilise these structural waters, while retaining their layer widening effect, is to co-intercalate another pillaring ion. Cao *et al.* demonstrated this in NIBs by pre-intercalating a  $\text{Y}^{3+}$  ion into hydrated  $\text{V}_2\text{O}_5$  to form  $\text{Y}_{0.02}\text{V}_2\text{O}_5$  and  $\text{Y}_{0.06}\text{V}_2\text{O}_5$  [30]. The  $\text{Y}^{3+}$  was observed to coordinate to the structural oxygen and the crystalline water to form  $[\text{YO}_6]$  octahedra, increasing the interlayer spacing from  $11.78 \text{ \AA}$  to  $12.03 \text{ \AA}$  and  $12.22 \text{ \AA}$  for  $\text{V}_2\text{O}_5$ ,  $\text{Y}_{0.02}\text{V}_2\text{O}_5$  and  $\text{Y}_{0.06}\text{V}_2\text{O}_5$  respectively. This is an excellent example of the pillaring effect, as ideally, the pillaring species should be kept as minimal as possible, as too many pre-intercalated species can start to block active sites that can be used by the charge carriers. This is what was observed for the increasing amount of  $\text{Y}^{3+}$ ,

as  $\text{Y}_{0.02}\text{V}_2\text{O}_5$  and  $\text{Y}_{0.06}\text{V}_2\text{O}_5$  were cycled for 100 cycles and retained 119 and 95  $\text{mAh g}^{-1}$  respectively, showing greater stability than the control  $\text{V}_2\text{O}_5$  that retained 84  $\text{mAh g}^{-1}$ . The pre-intercalated  $\text{Y}_x\text{V}_2\text{O}_5$  are also noticeably more consistent in cycling performance, likely due to the stabilisation of the water molecules by the  $\text{Y}^{3+}$ . The improvement shown by  $\text{Y}_{0.02}\text{V}_2\text{O}_5$  can be attributed clearly to the pre-intercalated  $\text{Y}^{3+}$  stabilising the lattice structure and preventing irreversible phase transitions that occur in pristine  $\text{V}_2\text{O}_5$ . The pre-intercalation of  $\text{Al}^{3+}$  is another popular method for stabilizing the  $\text{V}_2\text{O}_5$  structure, forming hydrogen aluminium vanadium oxide (HAVO). By altering the amount of  $\text{Al}^{3+}$  in between the VO layers, Mai *et al.* demonstrated for aqueous ZIBs that there is indeed a concentration dependent relationship for pre-intercalated ions [64]. When the mass ratio of Al:V was 1:16 or above 1:20, cycling performance and capacity were reduced. However, at 1:18, excellent stability and capacity were observed, retaining 252.9  $\text{mAh g}^{-1}$  after 3000 cycles at 1 A  $\text{g}^{-1}$ . This was supported by XRD analysis of the charge-discharge cycles, where minimal peak shifts or new peaks were observed in either *ex-situ* or *in-situ* XRD. The (001) peak shifted slightly to a higher  $2\theta$  angle, but the change was minimal. This is in sharp contrast to other *in-situ* work on un-pre-intercalated work, that observed both peak shifts, indicating lattice parameter shifts via intercalation, and new peaks appearing, indicating phase changes [65]. This superb structural stability and good capacity retention on cycling indicate that  $\text{Al}^{3+}$  can pillar effectively in  $\text{V}_2\text{O}_5$ , but also that over pre-intercalating can have detrimental effects to both

capacity and cycling stability. It was posited that a high Al:V ratio blocked channels in the structure, reducing diffusion more than the expansion of the interlayer spacing helped diffusion, thus requiring a balance.

Tunnel-type manganese dioxides are well known to suffer from significant capacity fading in ZIBs, due to phase transitions during  $\text{Zn}^{2+}$  insertion, collapsing the structure and inactivation of the tunnels, in addition to the Jahn–Teller effect of  $\text{Mn}^{3+}$  bringing additional structural distortion. To remain active, these tunnels require stabilisation. Pre-intercalation is well suited for this, as the pre-intercalating metal cations can stabilise the tunnels via the strong MO bonds that they form, along with providing doping energy levels, enhancing electronic conductivity. Yan *et al.* described  $\text{Al}^{3+}$  pre-intercalation to stabilise  $\alpha\text{-MnO}_2$  as a cathode for ZIBs [37]. By observing a shift in the (211) plane to lower angles after pre-intercalation, it was concluded that the  $\text{Al}^{3+}$  intercalated into the tunnels, expanding them through multiple M–O bonds. DFT calculations suggested that the pre-intercalated  $\text{Al}^{3+}$  resulted in  $\text{Mn}^{4+}$  reduction, lengthening the Mn–O bond, resulting in a wider and thus more favourable channels for  $\text{Zn}^{2+}$  diffusion. This was observed experimentally as Mn satellite peaks were present in the XPS spectra. The  $\text{Al}^{3+}$  was also observed to prevent the dissolution of manganese into the electrolyte, a common problem with manganese-based materials, as the stronger Al–O–Mn bonds stabilised the structure [24]. The stabilisation of  $\text{Al}^{3+}$  is further demonstrated by Lin *et al.* who synthesised  $\text{V}_2\text{O}_5$  with a dual pre-intercalation strategy using benzoquinone and  $\text{Al}^{3+}$  for ZIBs [27]. With the

benzoquinone alone, the stability was adequate, dropping by around 30% over 500 cycles. However, with the addition of electrochemically pre-intercalated  $\text{Al}^{3+}$ , the retained capacity is nearly 100%, which was attributed to the  $\text{Al}^{3+}$  insertion stabilising the  $\text{V}_2\text{O}_5$  structure. In addition, the co-intercalation of  $\text{Al}^{3+}$  was observed to suppress formation of  $\text{Zn}_3(\text{OH})_2\text{V}_2\text{O}_7 \cdot 2\text{H}_2\text{O}$ , which appears as rose-like nanosheets and is thought to reduced cyclability, so by supressing this phase, improvements to cyclability were observed. The strong Al–O–M bonds prevent local structural deformations, reducing phase transitions. As mentioned previously, this effect is a valuable area of further study.

Overall, pre-intercalation is well proven within the literature to efficiently improve cycling performance by limiting structural deformation and preventing phase changes via the pillaring effect. By pre-intercalating a larger species than the charge carriers, the lattice can be stabilised and its expansion and contraction on intercalation/de-intercalation can be reduced, sometimes even eliminated. However, restraint must be used when using pre-intercalation in this manner, as commonly observed is that excessive pre-intercalation can have adverse effects on both stability and capacity, either by occupying active sites that charge carriers could occupy, or by blocking channels that they would use to diffuse through the structure. In addition, to pillar effectively, the pre-intercalated species should be as minimally labile in the structure as possible, as it can contaminate and poison the electrolyte, increase side reactions or damaging the electrode structure when

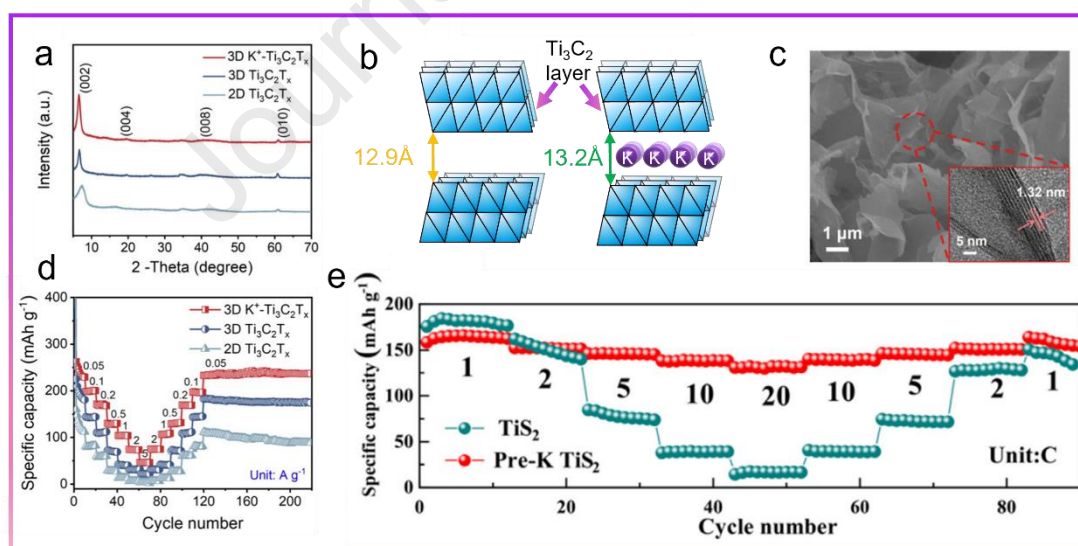
de-intercalating. Pre-intercalation is an excellent strategy for improving the cycling performance of materials.

### 3.3 Widening and Activation of Ionic Diffusion Channels

One of the most industrially important parameters is a materials rate performance. Fast charging has been deemed a key metric by the United States Advanced Battery Consortium (USABC), setting a 80% SOC within 15 mins goal for 2025 [66]. The largest roadblock to this target is the diffusion of ions within an active material in a short timeframe. The ionic conductivity of common carbonate electrolytes range from 3.1 to 36.7 mS cm<sup>-1</sup>, whereas ion diffusion coefficients in materials is often  $\sim 10^{-12}$  m<sup>2</sup> s<sup>-1</sup>, suggesting ionic diffusion in the material is the limiting factor [67]. Pre-intercalation can help alleviate this discrepancy, by increasing the distance between the layers, not only is more space provided to the charge carriers, but the coulombic interactions with the negatively charged layers is also reduced as the interaction decreases with the square of the distance, as per coulombs law. The improved ionic diffusion is commonly measured through two methods. Electrochemical impedance spectroscopy (EIS) allows for the direct measurement of the diffusion coefficient of ions through the analysis of the Warburg diffusion [68]. While less direct than EIS, rate performance is another valuable measurement method for ionic diffusion. As the ionic diffusion is the limiting factor, improvement to it will be most pronounced at higher rates. Titanium MXenes are an excellent candidate for high-rate electrode materials [69]. Their high electronic and ionic



conductivity compared to metal oxides allows for facile transport of ions and electrons. They can be further improved via pre-intercalation, as molybdenum has been pre-intercalated into titanium MXenes for LIBs, showing a significant rate performance increase [70]. Wang *et al.* pre-intercalated  $K^+$  into  $Ti_3C_2T_x$  to form  $K^+-Ti_3C_2T_x$ , as a high rate  $K$ -ion hybrid capacitor [71]. The rate performance was significantly improved, retaining  $40.3 \text{ mAh g}^{-1}$  at  $5 \text{ A g}^{-1}$ , compared to the controls (Fig. 8d). This was attributed to the larger interlayer distance, which from XRD was expanded from  $12.9 \text{ \AA}$  to  $13.2 \text{ \AA}$  (Fig. 8a–c), which allowed for the faster diffusion of ions through the 3D structure. An additional benefit was that the pillaring  $K^+$  ions also prevented significant restacking of the MXene sheets, a common issue with exfoliated layered materials [72].



**Fig. 8.** (a) XRD patterns of  $Ti_3C_2T_x$ , crumpled  $Ti_3C_2T_x$  and  $K^+-Ti_3C_2T_x$ . (b) Schematic representing the effects of pre-intercalating  $K^+$  in the interlayer spacing. (c) TEM image displaying the (002) plane. (d) The rate performance of  $Ti_3C_2T_x$ , crumpled  $Ti_3C_2T_x$  and  $K^+-Ti_3C_2T_x$  from  $50 \text{ mA g}^{-1}$  to  $5 \text{ A g}^{-1}$ . Reproduced with permission from Ref. [71]. Copyright © 2021 Wiley-VCH GmbH. (e) Rate performance of  $TiS_2$  and pre-intercalated  $K$ - $TiS_2$  from 1C to 20C. Reproduced with permission from Ref. [73]. Copyright © 2022 Published

by Elsevier Ltd on behalf of the editorial office of Journal of Materials Science & Technology.

In addition to improved capacity and cycling stability, vanadium oxides also show improved rate performance with upon pre-intercalation. Shao *et al.* reported carbon-coated calcium pre-intercalated  $V_2O_5$  ( $Ca_{0.34}V_2O_5$ ) nanoribbons as an anode for NIBs [61]. The calcium ions were shown via XRD and Rietveld refinement to be pillaring between the VO layers, expanding the interlayer spacing to 10.68 Å and stabilising the crystalline water. The  $Ca_{0.34}V_2O_5$  and carbon coated variation showed improved rate performance over other reported values for  $V_2O_5$ . Interestingly, there was observed to be a phase change during the initial charge and discharge, with the  $Ca^{2+}$  stabilising a metastable intermediary structure, resulting in final structure that can reversibly store  $Na^+$  without reverting to its initial state. Without the calcium pillaring and stabilising the intermediary phase, the structure would collapse and result in large irreversible capacity. Another promising material for fast rate charging in NIBs is  $TiS_2$ , but as before regarding the stability, its rate performance is also hampered by the large ionic radii of the post-Li ions. To address this, Shu *et al.* electrochemically pre-intercalated  $K^+$  into commercial  $TiS_2$ , expanding the interlayer spacing from 5.72 Å to 6.94 Å [73]. This expanded interlayer spacing translated into a hugely improved rate performance in NIBs for the K- $TiS_2$ , achieving 132.1 mAh g<sup>-1</sup> at 20 C, whereas the commercial  $TiS_2$  only achieved 16.4 mAh g<sup>-1</sup> (Fig. 8e). In addition, the diffusion coefficient was estimated via galvanostatic intermittent titration technique (GITT) during charge and

711 discharge, showing that the  $D_{Na^+}$  for the K-TiS<sub>2</sub> was consistently higher than  
712 TiS<sub>2</sub>,  $10^{-7}$ – $10^{-12}$  for K-TiS<sub>2</sub> and  $10^{-9}$ – $10^{-13}$  for TiS<sub>2</sub>. Although ICP-OES was said  
713 to be performed, no quantification of K content was contained, most likely due  
714 to the electrochemical synthesis method also intercalating K<sup>+</sup> into the  
715 surrounding conductive carbon, making quantification challenging. However,  
716 EDS was performed on samples after 500 cycles, with the result indicating that  
717 the K<sup>+</sup> remained in the structure, pillaring effectively without deintercalating  
718 during cycling. The effect of pre-intercalation on rate performance was also  
719 demonstrated in ZIBs with a dual pre-intercalation of Cs<sup>+</sup> and Na<sup>+</sup> by Zhang *et*  
720 *al.* into V<sub>2</sub>O<sub>5</sub>, forming monoclinic Na<sub>0.33</sub>V<sub>2</sub>O<sub>5</sub> and Na<sub>0.33</sub>Cs<sub>0.03</sub>V<sub>2</sub>O<sub>5</sub> [74]. These  
721 both display layered structures that have 1D tunnels for intercalation of charge  
722 carriers, providing an interesting case of the effect of pre-intercalation on  
723 tunnelled structures, rather than purely layered. The inclusion of Cs<sup>+</sup> in the  
724 structure, was observed to expand the interlayer spacing of the (100) plane to  
725 9.481 Å, from 9.342 Å with Na<sub>0.33</sub>V<sub>2</sub>O<sub>5</sub>, increasing the size of the tunnels. This  
726 was observed to improve rate performance, where the Na<sub>0.33</sub>Cs<sub>0.03</sub>V<sub>2</sub>O<sub>5</sub>  
727 outperformed the Na<sub>0.33</sub>V<sub>2</sub>O<sub>5</sub> by retaining 46.1% of the capacity at 5 A g<sup>-1</sup> that it  
728 achieved at 0.1 A g<sup>-1</sup> (376.5 mAh g<sup>-1</sup>), vs only 21.8% for Na<sub>0.33</sub>V<sub>2</sub>O<sub>5</sub>. Zhang *et*  
729 *al.* also performed GITT to investigate the diffusion coefficient of Zn<sup>2+</sup> within  
730 the structures, which was observed to be superior with pre-intercalated Cs<sup>+</sup> at all  
731 SOC, varying from  $\sim 5 \times 10^{-10}$  to  $\sim 1 \times 10^{-10}$  cm<sup>2</sup> s<sup>-1</sup>. As the structure is not the  
732 typical layered type, with instead channels for ion diffusion, it is interesting that

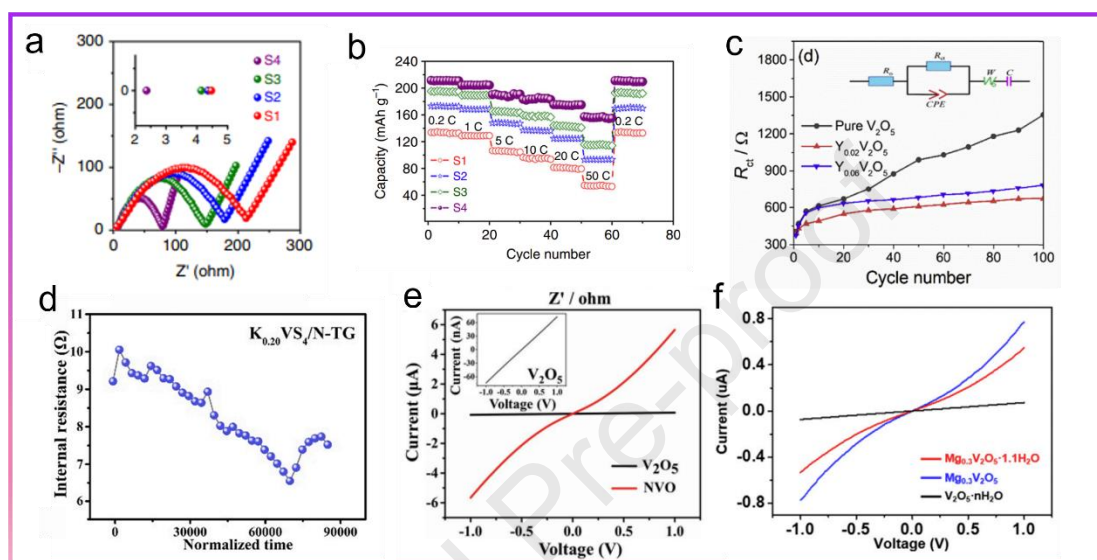
the pre-intercalation of the larger cation did not result in significant channel blockages, which would significantly reduce capacity and rate performance, particularly as larger cations are inherently less labile. Lastly, Mai *et al.* demonstrated the performance of hydrated pre-magnesi-ated vanadium oxide,  $\text{Mg}_{0.3}\text{V}_2\text{O}_5 \cdot 1.1 \text{ H}_2\text{O}$  in MIBs, comparing it to the hydrated  $\text{V}_2\text{O}_5$  and un-hydrated  $\text{Mg}_{0.3}\text{V}_2\text{O}_5$  [75]. Without interstitial  $\text{H}_2\text{O}$ , the  $\text{Mg}_{0.3}\text{V}_2\text{O}_5$  exhibited the smallest interlayer spacing and did not exhibit a bi-layered structure, leading to significantly impaired capacity and rate performance. However, a synergistic effect was observed with magnesium and water pre-intercalation, with it exhibiting a rate performance of retaining 80% of the initial capacity at  $2 \text{ A g}^{-1}$ ,  $85 \text{ mAh g}^{-1}$ , compared to  $\sim 30 \text{ mAh g}^{-1}$  for hydrated  $\text{V}_2\text{O}_5$  and  $\sim 20 \text{ mAh g}^{-1}$  for  $\text{Mg}_{0.3}\text{V}_2\text{O}_5$ . The additional stabilisation of the pillaring  $\text{Mg}^{2+}$ , combined with the water expanding the interlayer spacing to sufficiently accommodate the intercalating  $\text{Mg}^{2+}$  was the hypothesised reason for the improved rate performance. In summary, pre-intercalation is well suited to improve rate performance, as by pre-intercalating pillaring species, the  $d$ -spacing can be optimised to allow for the fastest diffusion of ions. By holding the layers apart at most commonly a larger  $d$ -spacing, the interactions of the intercalation ions with the lattice can be reduced, thus speeding up their diffusion throughout the structure. Counter examples do exist, where a reduction in lattice spacing increases the rate, but these are structures with already large absolute  $d$ -spacings, indicating optimisation is more important than absolute distance.

### 3.4 Introduction of Dopants

The electronic conductivity of transition metal oxide electrode materials is often poor, as the weakly held valence electrons that formed the conduction band of the metal centres have now been covalently bonded with the oxygen groups, preventing electron delocalisation and thus reduced conductivity [76]. Commonly, the conductivity of metal oxides in the energy storage literature is improved extrinsically, specifically through carbon coating [77]. This can greatly improve the rate performance and capacity of the material but results in a greater percentage of carbon in the electrode, leading to a thick SEI formation and poor cycling performance [78, 79]. By altering a material's inherent conductivity, rate performance and potential capacity can be further improved. This can be achieved via pre-intercalation, as by pre-intercalating charged species, some of the metal centres are reduced, resulting in additional levels in the band-gap, allowing for the promotion of electrons and the creation of charge carrying holes or electrons in the valence band or conduction band respectively [80]. While this process would occur eventually with the intercalation of charge carriers during cycling, by tuning the pre-intercalation level, the number of additional doping levels provided by the pre-intercalated species can also be increased. In addition, the introduction of additional species in the interlayer spacing can result in n-type doping, where the additional electrons from the pre-intercalated species can be donated to the structure, resulting in enhanced electronic conductivity. Direct

measures of electronic conductivity are rare but can be estimated from a direct relationship to the charge transfer resistance ( $R_{ct}$ ) of EIS measurements [81]. Meng *et al.* reported  $\text{Na}^+$  pre-intercalated Birnessite and monoclinic manganese oxides for NIBs, which provided an excellent example of the level of pre-intercalation effecting the conductivity of the material [82]. The measured  $R_{ct}$  of  $\text{Na}_{0.46}\text{MnO}_{2-y}(\text{OH})_{2y} \cdot 0.61 \text{ H}_2\text{O}$ ,  $\text{Na}_{0.71}\text{MnO}_{2-y}(\text{OH})_{2y} \cdot 0.32 \text{ H}_2\text{O}$  and  $\text{NaMnO}_{2-y}(\text{OH})_{2y} \cdot 0.10 \text{ H}_2\text{O}$  was improved with the increasing  $\text{Na}^+$  pre-intercalation, from  $\sim 225 \Omega$  to  $\sim 150 \Omega$  (Fig. 9a). This was then carried over into the performance, with the monoclinic  $\text{NaMnO}_{2-y}(\text{OH})_{2y} \cdot 0.10 \text{ H}_2\text{O}$ , denoted as S3, outperforming the both the other samples in both capacity and rate performance (Fig. 9b). The final sample (S4) included oxygen vacancies, which was the ascribed reason for the improved electronic conductivity. However, the other samples showed increasing electronic conductivity without the vacancies, so much of the improved electronic conductivity must have come from the level of pre-intercalated  $\text{Na}^+$ , but requires further work and direct conductivity measurements to confirm. Meng *et al.* continued utilising this effect to improve the electronic conductivity of  $\text{VS}_4$ / nitrogen doped tubular graphene (N-TG), by electrochemically pre-intercalating  $\text{K}^+$  into the layers [83]. Observed was a significant reduction in the internal resistance compared to pristine  $\text{VS}_4$ /N-TG, with an average resistance of  $8 \Omega$  vs  $15 \Omega$  (Fig. 9d). As the internal resistance includes charge transfer resistance, it was concluded that pre-intercalated  $\text{K}^+$  improved the electronic conductivity of the  $\text{VS}_4$ . The effect of increasing a pre-

intercalated species was further investigated by Cao *et al.* using the  
 aforementioned  $Y_xV_2O_5$ , where they investigated the  $R_{ct}$  of  $V_2O_5$  with varying  
 degrees of Y pre-intercalation for NIBs (Fig. 9c) [30].



**Fig. 9.** (a) EIS measurement of  $Na_{0.46}MnO_{2-y}(OH)_{2y} \cdot 0.61 H_2O$  (S1),  $Na_{0.71}MnO_{2-y}(OH)_{2y} \cdot 0.32 H_2O$  (S2) and  $NaMnO_{2-y}(OH)_{2y} \cdot 0.10 H_2O$  (S3). (b) Rate performance of  $Na_{0.46}MnO_{2-y}(OH)_{2y} \cdot 0.61 H_2O$  (S1),  $Na_{0.71}MnO_{2-y}(OH)_{2y} \cdot 0.32 H_2O$  (S2) and  $NaMnO_{2-y}(OH)_{2y} \cdot 0.10 H_2O$  (S3) from 0.2C to 50C. Reproduced with permission from Ref. [82]. Copyright © 2018, Hui Xia *et al.* (c) Comparison of  $R_{ct}$  over cycling for  $V_2O_5$ ,  $Y_{0.02}V_2O_5$  and  $Y_{0.06}V_2O_5$ . Reproduced with permission from Ref. [30]. Copyright © 2018 Elsevier Ltd. All rights reserved. (d) Calculated internal resistance of  $K_{0.2}VS_4/N-TG$ . Copyright © 2021 Elsevier Ltd. All rights reserved. (e) I-V curves of  $V_2O_5$  and  $Na_{0.33}V_2O_5$ . Reproduced with permission from Ref. [84]. Copyright © 2018 WILEY-VCH Verlag GmbH & Co. KGaA, Weinheim. (f) I-V curves of  $Mg_{0.3}V_2O_5 \cdot 1.1 H_2O$ ,  $Mg_{0.3}V_2O_5$  and  $V_2O_5 \cdot n H_2O$ . Reproduced with permission from Ref. [75]. Copyright © 2019 Elsevier Inc.

What was observed contradicts the result from Meng *et al.* as when the yttrium  
 content was increased from  $x = 0.02$  to  $x = 0.06$ , the  $R_{ct}$  increases to  $\sim 700 \Omega$ ,  
 from  $\sim 600 \Omega$ . This indicates that increasing the pre-intercalated species may not  
 always be beneficial to conductivity, as generally a large number of dopants can



result in a more impeded path for the electrons, as in this case the yttrium ions can pull charge density away from the lattice, reducing charge carriers and thus creating a non-linear doping effect. While yttrium is a rather unique pre-intercalated ion,  $\text{Na}^+$  pre-intercalated vanadium oxide nanowires,  $\text{Na}_{0.33}\text{V}_2\text{O}_5$  was investigated by Mai *et al.* for ZIBs [84]. The  $\text{Na}^+$  ions induced  $\text{V}^{4+}$  vacancies in the  $\text{V}^{5+}$  lattice, resulting in a conductivity of  $5.9 \times 10^4 \text{ S m}^{-1}$ , compared to pristine  $\text{V}_2\text{O}_5$  with a conductivity of  $7.3 \text{ S m}^{-1}$  (Fig. 9e). This was also confirmed in the EIS, with  $\text{Na}_{0.33}\text{V}_2\text{O}_5$  displaying an  $R_{\text{ct}}$  of  $5.6 \Omega$  after the first cycle, vs  $8.7 \Omega$  for  $\text{V}_2\text{O}_5$ . This improved electronic conductivity translated to an improved rate performance, with the  $\text{Na}_{0.33}\text{V}_2\text{O}_5$  retaining  $96.4 \text{ mAh g}^{-1}$  at  $2 \text{ A g}^{-1}$ . As before, this indicates that the pre-intercalation of charged ions inducing valences changes in small numbers of redox active metal centers is beneficial to conductivity, which in turn improves electrochemical performance. This is further evidenced by another work by Mai *et al.*, as they investigated magnesium pre-intercalated bi-layered vanadium oxide,  $\text{Mg}_{0.3}\text{V}_2\text{O}_5 \cdot 1.1 \text{ H}_2\text{O}$  for MIBs [75]. When compared to the bi-layered  $\text{V}_2\text{O}_5 \cdot n \text{ H}_2\text{O}$  control, the conductivity is significantly improved, from  $10.1 \text{ S m}^{-1}$  to  $5.0 \times 10^3 \text{ S m}^{-1}$  (Fig. 9f). The stabilising structural water was also attempted to be removed to form  $\text{Mg}_{0.3}\text{V}_2\text{O}_5$ , but the structure collapsed and while the electronic conductivity is improved, the structure was observed to not be conducive for ionic diffusion and thus the performance is reduced to only 200 cycles before failing, with below  $50 \text{ mAh g}^{-1}$  for most of the cycles.



Overall, pre-intercalation is a valuable tool for improving the inherent electronic conductivity of poorly conducting active materials. The combination of the introduction of additional dopant levels from the pre-intercalated species and the valence changes of the metal redox centres to provide additional levels within the band gap of these insulators or semiconductors can dramatically improve the initial conductivity of the material. However, this process will inevitably happen during the charge–discharge process, as to charge balance the incoming cations, a metal centre must accept an electron, creating a valence doped structure. However as discussed, even during different SOC, the pre-intercalated materials are still more conductive, implying that pre-intercalation amplifies this effect. Another cautionary aspect is that the pre-intercalation level should be thoughtfully considered, as over pre-intercalating or the removal of stabilizing species in favour of pre-intercalated species can have negative effects, despite having an improved conductivity.

#### 4. Perspectives and Outlook

Despite being one of the oldest techniques for altering the properties of intercalation-type battery materials, pre-intercalation has seen a resurgence in recent years and is rapidly proving to be a timely and impactful tool [42, 43].

By intelligently optimising the pre-intercalated species, namely its valence and size, along with the degree of pre-intercalation, the key properties of *d*-spacing, lattice stability with cycling and the level of doping by inducing valence changes in the metal redox centres can be positively altered. These correspond to

improvements in capacity, ionic and electronic conductivity, and have been proven repeatedly to be superior to the un-pre-intercalated materials. The benefits to this approach are numerous. Firstly, the alternations to the material are intrinsic, so any morphology optimisation and post-synthesis processing, such as carbon coating, can also be applied to pre-intercalated materials in addition, rather than in place of. Secondly, while many pre-intercalation syntheses can be criticised for their cost, use of toxic and unsustainable reagents and lack of control, equally as many are facile, cheap and sustainable, requiring only a small amount of the pre-intercalated species to be included in the synthesis or a simple aqueous ion-exchange post synthesis [30, 85, 86]. Thirdly, the level of pre-intercalation can be highly tuneable, allowing for a large degree of control over the final product, resulting in a highly specific product that can be directed for a specific merit of the product, e.g. high rate or high stability.

However, as with all tools, there are some pitfalls. Firstly, the lability of the pre-intercalated species must be cautiously considered, as during cycling, the partial or total de-intercalation of the pre-intercalated species is highly likely, if not certain. This can not only reduce the effect of the pre-intercalated species, but also cause poisoning of the electrolyte and opposite electrode, along with unwanted side reactions and destruction of the host lattice. Keeping this in mind, very labile species should be avoided to minimise this effect. Secondly, considerable restraint must also be employed with the degree of pre-intercalation, as too many pre-intercalated species can start blocking diffusion paths of the

charge carriers and occupying active sites, along with increasing the electrostatic interactions with the charge carriers, which increases electrostatic repulsions and reducing the storage capacity of the material.

For the outlook of the field, there are some distinctly fruitful avenues that require further investigation. Firstly, the pre-intercalation of redox active species could be a novel avenue, as none of the species mentioned in this review were demonstrated to be redox active, within their host structures. This could totally off-set the energy density reduction associated with pre-intercalation, while retaining the benefits of pre-intercalation, addressing a common criticism of pre-intercalation. Secondly, multi-species pre-intercalation could be a promising further development. Each species could be optimised to provide synergistic benefits to the host material, further enhancing the electrochemical performance. Thirdly, the relationship of  $d$ -spacing enlargement could be further investigated by a staging of multiple rounds of pre-intercalation, activating the lattice to further accommodate larger species. This would expand the  $d$ -spacing further, potentially enhancing electrochemical performance further. Fourthly, in the authors opinion, there is a significant research gap in investigating the structure of the pre-intercalated materials. The occupation sites of the pre-intercalated species and its local environment changes are almost never investigated, with often the only evidence given being the increase in  $d$ -spacing via XRD. A thorough investigation into the occupied sites and how these changes affect the mechanism of intercalation is sorely needed.

Finally, the benefits of pre-intercalation have been proven almost exclusively in a half-cell configuration, with no ion intercalation taking place at the metal counter electrode. Given the “Rocking chair” nature of rechargeable ion batteries, an investigation into the behaviour of the pre-intercalated species in a full-cell configuration would be of great value. Of particular interest, is the de-intercalation and re-intercalation of the pre-intercalated species from the working electrode into an intercalation based counter electrode, for which intercalation behaviour of the species and liability to full-cell performance are unclear. In the authors’ opinion, pre-intercalation research is an under-utilised aspect in the energy storage field. If continued research finds that the liability of the pre-intercalated species do not impose significant negatives, we believe that many materials could strongly benefit from the positives pre-intercalation provides. Also, the most convincing is the pillaring effect and its improvements to stability. A material that retains its stability, at both high and low rates, is essential for large-scale storage, which currently is a topical aspect of energy research. Pre-intercalation has concretely demonstrated that through careful and insightful choice of intercalation degree and species, the stability of materials can be dramatically improved.

#### **Author contributions**

Conceptualisation, C.A.F.N.; Writing – Original Draft, C.A.F.N.; Writing – Review & Editing, Y.X. and C.A.F.N.; Supervision and Funding Acquisition, Y.X. All authors participated in manuscript discussion.

## Competing financial interests

The authors declare no competing financial interests.

## Acknowledgments

Y.X. acknowledges the support of the Engineering and Physical Sciences Research Council (EP/V000152/1, EP/X000087/1), Leverhulme Trust (RPG-2021-138), and Royal Society (RGS\R2\212324, SIF\R2\212002, IEC\NSFC\223016). For the purpose of open access, the author has applied a Creative Commons Attribution (CC BY) licence to any Author Accepted Manuscript version arising.

## References

- [1] K. Mizushima, P. C. Jones, P. J. Wiseman, J. B. Goodenough,  $\text{Li}_x\text{CoO}_2$  ( $0 < x < 1$ ): A new cathode material for batteries of high energy density, *Mater. Res. Bull.* 15 (1980) 783-789.
- [2] G. Liu, Z. Zhao, A. Ghahreman, Novel approaches for lithium extraction from salt-lake brines: A review, *Hydrometallurgy* 187 (2019) 81-100.
- [3] London Metals Exchange (Accessed Nov 2022).
- [4] R. P. Ramasamy, Toward a least-effort principle for evaluating prices of elements as indicators of sustainability, *MRS Energy Sustain.* 8 (2021) 16–32.
- [5] A. Konarov, H. J. Kim, H. Yashiro, S.-T. Myung, Passivation of aluminum current collectors in non-aqueous carbonate solutions containing sodium or potassium hexafluorophosphate salts, *J. Mater. Chem. A* 7 (2019) 13012-13018.
- [6] R. C. Asher, A lamellar compound of sodium and graphite, *J. Inorg. Nucl. Chem.* 10 (1959) 238-249.
- [7] S. Komaba, T. Hasegawa, M. Dahbi, K. Kubota, Potassium intercalation into graphite to realize high-voltage/high-power potassium-ion batteries and potassium-ion capacitors, *Electrochem. Commun.* 60 (2015) 172-175.
- [8] Y. Marcus, Thermodynamic functions of transfer of single ions from water to nonaqueous and mixed solvents: Part 3 - Standard potentials of selected electrodes, *Pure Appl. Chem.* 57 (1985) 1129-1132.
- [9] CRC Handbook of Chemistry and Physics. 97th ed 2016-2017.
- [10] A. Eftekhari, Potassium secondary cell based on Prussian blue cathode, *J. Power Sources.* 126 (2004) 221-228.
- [11] V. Gabaudan, L. Monconduit, L. Stievano, R. Berthelot, Snapshot on negative electrode materials for potassium-ion Batteries, *Front. Energy Res.* 7 (2019) 46.
- [12] H. Li, C. Han, Y. Huang, Y. Huang, M. Zhu, Z. Pei, Q. Xue, Z. Wang, Z. Liu, Z. Tang, Y. Wang, F. Kang, B. Li, C. Zhi, An extremely safe and wearable solid-state zinc ion battery based on a hierarchical structured polymer electrolyte, *Energy Environ. Sci.* 11 (2018) 941-951.

- 970 [13]Z. Zhao-Karger, M. Fichtner, Beyond intercalation chemistry for  
971 rechargeable Mg batteries: A short review and perspective, *Front Chem.* 6 (2018)  
972 656.
- 973 [14]W. L. Worrell, Electrochemical investigations of novel electrode materials.  
974 Progress report, November 1, 1981-December 31, 1982. Office of Scientific and  
975 Technical Information (OSTI); 1982.
- 976 [15]M. B. Armand. Intercalation Electrodes. In: Murphy DW, Broadhead J,  
977 Steele BCH, editors. *Materials for advanced batteries*. Boston, MA: Springer US;  
978 1980. p. 145-161.
- 979 [16]G. Demazeau, Solvothermal and hydrothermal processes: the main physico-  
980 chemical factors involved and new trends, *Res. Chem. Intermed.* 37 (2011) 107-  
981 123.
- 982 [17]D. Navas, S. Fuentes, A. Castro-Alvarez, E. Chavez-Angel, Review on sol-  
983 gel synthesis of perovskite and oxide nanomaterials, *Gels* 7 (2021) 275.
- 984 [18]M. Aykol, J. H. Montoya, J. Hummelshoj, Rational solid-state synthesis  
985 routes for inorganic materials, *J Am Chem Soc.* 143 (2021) 9244-9259.
- 986 [19]Y.-H. Luo, Q.-L. Pan, H.-X. Wei, Y.-D. Huang, L.-B. Tang, Z.-Y. Wang, C.  
987 Yan, J. Mao, K.-H. Dai, Q. Wu, X.-H. Zhang, J.-C. Zheng, Fundamentals of ion-  
988 exchange synthesis and its implications in layered oxide cathodes: Recent  
989 advances and perspective, *Adv. Energy Mater.* 13 (2023) 2300125.
- 990 [20]R. Uppuluri, A. Sen Gupta, A. S. Rosas, T. E. Mallouk, Soft chemistry of  
991 ion-exchangeable layered metal oxides, *Chem. Soc. Rev.* 47 (2018) 2401-2430.
- 992 [21]H. Chen, X. Qiu, W. Zhu, P. Hagenmuller, Synthesis and high rate properties  
993 of nanoparticled lithium cobalt oxides as the cathode material for lithium-ion  
994 battery, *Electrochem. Commun.* 4 (2002) 488-491.
- 995 [22]S. Park, J.-N. Chotard, D. Carlier, I. Moog, M. Duttine, F. Fauth, A. Iadecola,  
996 L. Croguennec, C. Masquelier, An asymmetric sodium extraction/insertion  
997 mechanism for the Fe/V-mixed NASICON  $\text{Na}_4\text{FeV}(\text{PO}_4)_3$ , *Chem. Mater.* 34  
998 (2022) 4142-4152.
- 999 [23]S. Park, J.-N. Chotard, D. Carlier, I. Moog, M. Courty, M. Duttine, F. Fauth,  
1000 A. Iadecola, L. Croguennec, C. Masquelier, Crystal structures and local  
1001 environments of NASICON-Type  $\text{Na}_3\text{FeV}(\text{PO}_4)_3$  and  $\text{Na}_4\text{FeV}(\text{PO}_4)_3$  positive  
1002 electrode materials for Na-ion batteries, *Chem. Mater.* 33 (2021) 5355-5367.
- 1003 [24]K. Li, J. Lv, T. Cao, Y. Gong, D. L. Zhang, Anthraquinone-intercalated  
1004  $\text{V}(\text{2})\text{O}(\text{5})$  with  $\text{Al}(\text{3+})$  for superior zinc-ion batteries: reversible transformation  
1005 between disorder and order, *Chem Commun.* 58 (2022) 12365-12368.
- 1006 [25]O. C. Gagne, F. C. Hawthorne, Bond-length distributions for ions bonded to  
1007 oxygen: alkali and alkaline-earth metals, *Acta Crystallogr. Sect. B: Struct. Sci.*  
1008 72 (2016) 602-625.
- 1009 [26]J. W. Steed, First- and second-sphere coordination chemistry of alkali metal  
1010 crown ether complexes, *Coord. Chem. Rev.* 215 (2001) 171-221.
- 1011 [27]K. Li, Y. Gong, J. H. Lin, Benzoquinone-intercalated vanadium oxide in the  
1012 electrolyte with  $\text{Al}^{3+}$  for zinc-ion storage: dual-pillar effect and reversible  
1013 disorder–order conversion, *Chem. Eng. J.* 452 (2023) 139621.

- [28]K. W. Hipps, U. Mazur, Electron affinity states of metal supported phthalocyanines measured by tunneling spectroscopy, *J. Porphyrins Phthalocyanines*. 16 (2012) 273-281.
- [29]P. Chomkhuntod, K. Hantanasirisakul, S. Duangdangchote, N. Phattharasupakun, M. Sawangphruk, The charge density of intercalants inside layered birnessite manganese oxide nanosheets determining Zn-ion storage capability towards rechargeable Zn-ion batteries, *J. Mater. Chem. A* 10 (2022) 5561-5568.
- [30]C. Liu, J. Yao, Z. Zou, Y. Li, G. Cao, Boosting the cycling stability of hydrated vanadium pentoxide by  $Y^{3+}$  pillaring for sodium-ion batteries, *Mater. Today Energy* 11 (2019) 218-227.
- [31]T. Jing, Y. Dai, X. Ma, W. Wei, B. Huang, Effects of intrinsic defects and extrinsic doping on the electronic and photocatalytic properties of  $Ta_3N_5$ , *RSC Adv.* 5 (2015) 59390-59397.
- [32]K. Kanetani, K. Sugawara, T. Sato, R. Shimizu, K. Iwaya, T. Hitosugi, T. Takahashi, Ca intercalated bilayer graphene as a thinnest limit of superconducting  $C_6Ca$ , *PNAS* 109 (2012) 19610-19613.
- [33]S. Tosoni, C. Di Valentin, G. Pacchioni, Effect of Alkali Metals Interstitial Doping on Structural and Electronic Properties of  $WO_3$ , *J. Phys. Chem. C* 118 (2014) 3000-3006.
- [34]G. V. Gibbs, F. C. Hill, M. B. Boisen, R. T. Downs, Power law relationships between bond length, bond strength and electron density distributions, *Phys. Chem. Miner.* 25 (1998) 585-590.
- [35]J. Zhang, L. Cheng, L. Ma, S. Sang, L. Xu, Y. Jiang,  $SiS_2$  monolayer: An auspicious alkali-ion anode material with high specific capacity and ultrafast ion diffusion. *Phys. E: Low-Dimens. Syst. Nanostructures*. 144 (2022) 115474.
- [36]J. L. Kaufman, J. Vinckevičiūtė, S. Krishna Kolli, J. Gabriel Goiri, A. Van der Ven, Understanding intercalation compounds for sodium-ion batteries and beyond, *Philos. Trans. Royal Soc. A PHILOS T R SOC A*. 377 (2019) 20190020.
- [37]C. Chen, M. Shi, Y. Zhao, C. Yang, L. Zhao, C. Yan, Al-Intercalated  $MnO_2$  cathode with reversible phase transition for aqueous Zn-ion batteries, *Chem. Eng. J.* 422 (2021) 130375.
- [38]Y. Wen, K. He, Y. Zhu, F. Han, Y. Xu, I. Matsuda, Y. Ishii, J. Cumings, C. Wang, Expanded graphite as superior anode for sodium-ion batteries, *Nat. Commun.* 5 (2014) 4033.
- [39]M. Tian, C. Liu, J. Zheng, X. Jia, E. P. Jahrman, G. T. Seidler, D. Long, M. Atif, M. Alsalihi, G. Cao, Structural engineering of hydrated vanadium oxide cathode by  $K^+$  incorporation for high-capacity and long-cycling aqueous zinc ion batteries, *Energy Stor. Mater.* 29 (2020) 9-16.
- [40]X. Zhang, Z. Zhang, S. Yao, A. Chen, X. Zhao, Z. Zhou, An effective method to screen sodium-based layered materials for sodium ion batteries, *Npj Comput. Mater.* 4 (2018) 13.
- [41]M. Feng, Q. Du, L. Su, G. Zhang, G. Wang, Z. Ma, W. Gao, X. Qin, G. Shao, Manganese oxide electrode with excellent electrochemical performance for



- sodium ion batteries by pre-intercalation of K and Na ions, *Sci Rep.* 7 (2017) 2219.
- [42]X. Yao, Y. Zhao, F. A. Castro, L. Mai, Rational Design of Preintercalated Electrodes for Rechargeable Batteries, *ACS Energy Lett.* 4 (2019) 771-778.
- [43]Y. Liu, J. Xu, J. Li, Z. Yang, C. Huang, H. Yu, L. Zhang, J. Shu, Pre-intercalation chemistry of electrode materials in aqueous energy storage systems, *Coord. Chem. Rev.* 460 (2022) 214477.
- [44]Q. Liu, F. Han, J. Zhou, Y. Li, L. Chen, F. Zhang, D. Zhou, C. Ye, J. Yang, X. Wu, J. Liu, Boosting the potassium-ion storage performance in soft carbon anodes by the synergistic effect of optimized molten salt medium and N/S dual-doping. *ACS Appl. Mater. Interfaces* 12 (2020) 20838-20848.
- [45]C. Liu, N. Xiao, H. Li, Q. Dong, Y. Wang, H. Li, S. Wang, X. Zhang, J. Qiu, Nitrogen-doped soft carbon frameworks built of well-interconnected nanocapsules enabling a superior potassium-ion batteries anode, *Chem. Eng. J.* 382 (2020) 121759.
- [46]K.-H. Nam, V. Ganesan, K. H. Chae, C.-M. Park, High-performance carbon by amorphization and prepotassiation for potassium-ion battery anodes, *Carbon* 181 (2021) 290-299.
- [47]S. Tepavcevic, H. Xiong, V. R. Stamenkovic, X. Zuo, M. Balasubramanian, V. B. Prakapenka, C. S. Johnson, T. Rajh, Nanostructured Bilayered Vanadium Oxide Electrodes for Rechargeable Sodium-Ion Batteries, *ACS Nano* 6 (2012) 530-538.
- [48]Q. Ren, N. Qin, B. Liu, Y. Yao, X. Zhao, Z. Deng, Y. Li, Y. Dong, D. Qian, B.-L. Su, W. Zhang, H.-E. Wang, An oxygen-deficient vanadium oxide@N-doped carbon heterostructure for sodium-ion batteries: insights into the charge storage mechanism and enhanced reaction kinetics, *J. Mater. Chem. A* 8 (2020) 3450-3458.
- [49]J. Song, S. Park, S. Kim, V. Mathew, M. H. Alfaruqi, J. Jo, J. Kim, Uniform Carbon coated  $\text{Na}_3\text{V}_2(\text{PO}_4)_2\text{O}_{2x}\text{F}_{3-2x}$  nanoparticles for sodium ion batteries as cathode, *ACS Sustain. Chem. Eng.* 7 (2019) 18826-18834.
- [50]M. Clites, B. W. Byles, E. Pomerantseva, Effect of aging and hydrothermal treatment on electrochemical performance of chemically pre-intercalated Na-V-O nanowires for Na-ion batteries, *J. Mater. Chem. A* 4 (2016) 7754-7761.
- [51]D. Su, G. Wang, Single-crystalline bilayered  $\text{V}_2\text{O}_5$  nanobelts for high-capacity sodium-ion batteries. *ACS Nano* 7 (2013) 11218-11226.
- [52]V. Raju, J. Rains, C. Gates, W. Luo, X. Wang, W. F. Stickle, G. D. Stucky, X. Ji, Superior cathode of sodium-ion batteries: orthorhombic  $\text{V}_2\text{O}_5$  nanoparticles generated in nanoporous carbon by ambient hydrolysis deposition, *Nano Lett.* 14 (2014) 4119-4124.
- [53]M. Clites, J. L. Hart, M. L. Taheri, E. Pomerantseva, Chemically preintercalated bilayered  $\text{K}_x\text{V}_2\text{O}_5 \cdot n\text{H}_2\text{O}$  nanobelts as a high-performing cathode material for K-ion batteries, *ACS Energy Lett.* 3 (2018) 562-567.

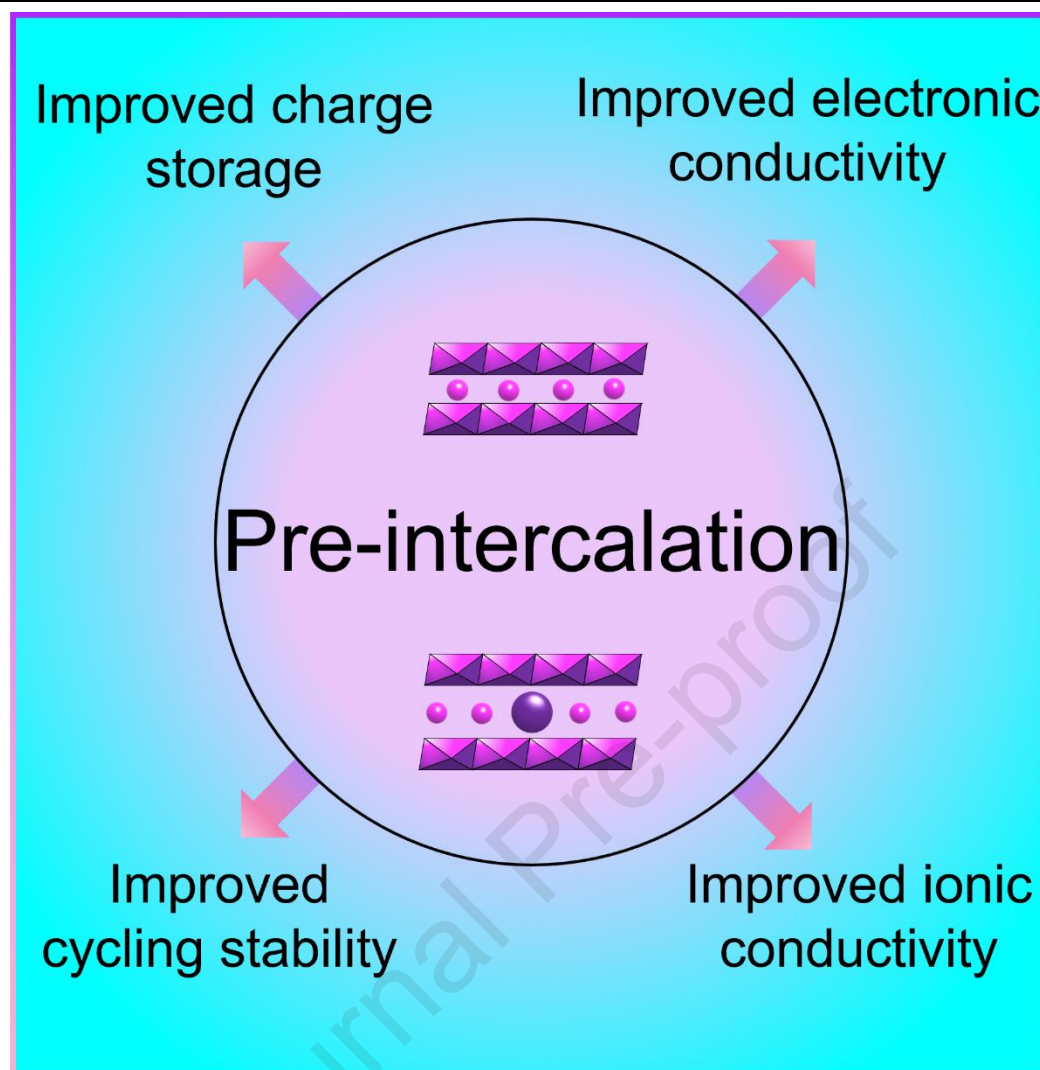


- [54]D. S. Charles, M. Feyngenson, K. Page, J. Neuefeind, W. Xu, X. Teng, Structural water engaged disordered vanadium oxide nanosheets for high capacity aqueous potassium-ion storage, *Nat Commun.* 8 (2017) 15520.
- [55]Q. Xie, G. Cheng, T. Xue, L. Huang, S. Chen, Y. Sun, M. Sun, H. Wang, L. Yu, Alkali ions pre-intercalation of  $\delta$ -MnO<sub>2</sub> nanosheets for high-capacity and stable Zn-ion battery, *Mater. Today Energy.* 24 (2022) 100934.
- [56]X. Wang, P. Hu, C. Niu, J. Meng, X. Xu, X. Wei, C. Tang, W. Luo, L. Zhou, Q. An, L. Mai, New-type K<sub>0.7</sub>Fe<sub>0.5</sub>Mn<sub>0.5</sub>O<sub>2</sub> cathode with an expanded and stabilized interlayer structure for high-capacity sodium-ion batteries, *Nano Energy* 35 (2017) 71-78.
- [57]Y. Zhao, C. Han, J. Yang, J. Su, X. Xu, S. Li, L. Xu, R. Fang, H. Jiang, X. Zou, B. Song, L. Mai, Q. Zhang, Stable alkali metal ion intercalation compounds as optimized metal oxide nanowire cathodes for lithium batteries, *Nano Lett.* 15 (2015) 2180-2185.
- [58]M. S. Whittingham, Electrical energy storage and intercalation chemistry, *Science* 192 (1976) 1126-1127.
- [59]G. L. Holleck, J. R. Driscoll, Transition metal sulfides as cathodes for secondary lithium batteries—II. titanium sulfides, *Electrochim. Acta.* 22 (1977) 647-655.
- [60]B. Tian, W. Tang, K. Leng, Z. Chen, S. J. R. Tan, C. Peng, G.-H. Ning, W. Fu, C. Su, G. W. Zheng, K. P. Loh, Phase transformations in TiS<sub>2</sub> during K intercalation, *ACS Energy Lett.* 2 (2017) 1835-1840.
- [61]Y. Tang, H. Zhang, S. Zhang, L. Li, Z. Liu, Z. Li, J. Shen, H. Shao, High performance anode for sodium-ion batteries: Calcium pre-intercalated layered vanadium oxide/carbon composite, *Chem. Eng. J.* 424 (2021) 130378.
- [62]Y. Fan, Z. Qu, W. Zhong, Z. Hu, H. A. Younus, C. Yang, X. Wang, S. Zhang, Understanding the effect of interplanar space and preintercalated cations of vanadate cathode materials on potassium-ion battery performance, *ACS Appl. Mater. Interfaces* 13 (2021) 7377-7388.
- [63]B. Tian, W. Tang, C. Su, Y. Li, Reticular V<sub>2</sub>O<sub>5</sub>·0.6H<sub>2</sub>O xerogel as cathode for rechargeable potassium ion batteries, *ACS Appl. Mater. Interfaces* 10 (2018) 642-650.
- [64]L. Xing, C. Zhang, M. Li, P. Hu, X. Zhang, Y. Dai, X. Pan, W. Sun, S. Li, J. Xue, Q. An, L. Mai, Revealing excess Al<sup>3+</sup> preinsertion on altering diffusion paths of aluminum vanadate for zinc-ion batteries, *Energy Stor. Mater.* 52 (2022) 291-298.
- [65]P. Jing, W. Wei, W. Luo, X. Li, F. Xu, H. Li, M. Wei, D. Yu, Q. Zhu, G. Liu, In-situ XRD study of the structure and electrochemical performance of V<sub>2</sub>O<sub>5</sub> nanosheets in aqueous zinc ion batteries, *Inorg. Chem. Commun.* 117 (2020) 107953.
- [66]A. Masias, J. Marcicki, W. A. Paxton, Opportunities and challenges of lithium ion batteries in automotive applications, *ACS Energy Lett.* 6 (2021) 621-630.

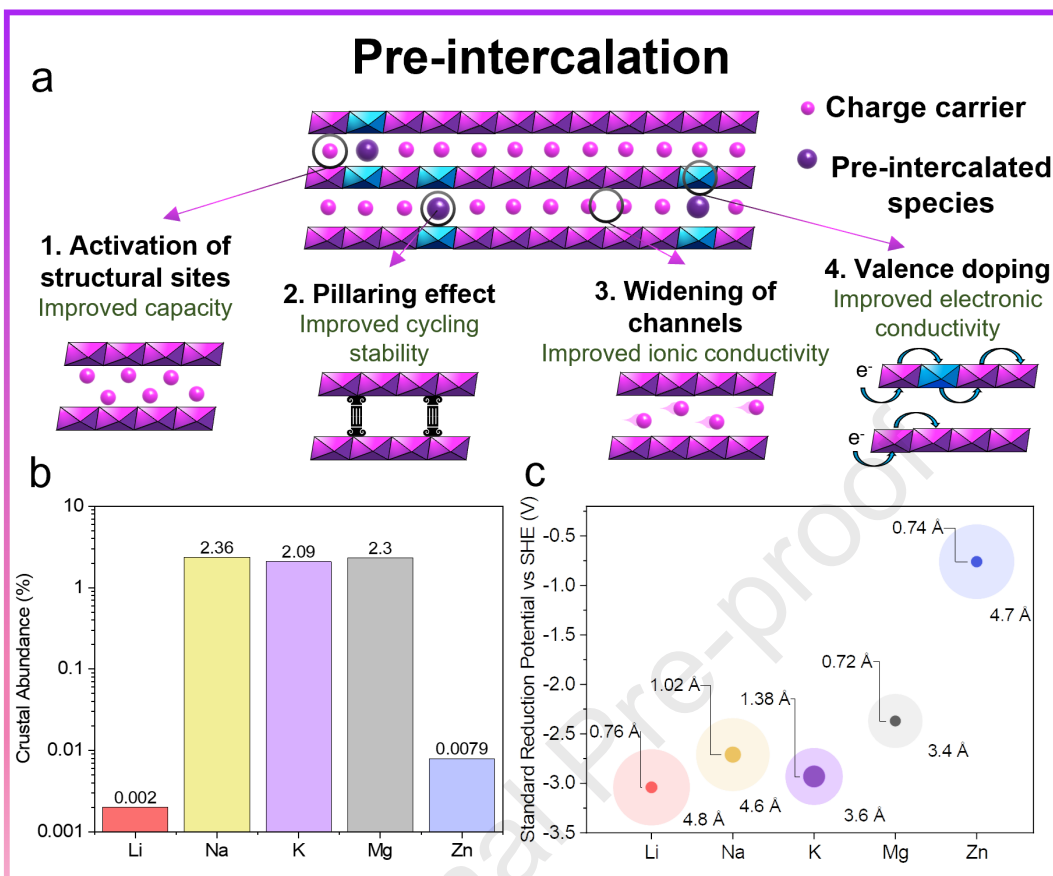
- [67]M. Zhou, P. Bai, X. Ji, J. Yang, C. Wang, Y. Xu, Electrolytes and interphases in potassium ion batteries. *Adv Mater.* 33 (2021) e2003741.
- [68]J. Huang, Diffusion impedance of electroactive materials, electrolytic solutions and porous electrodes: Warburg impedance and beyond, *Electrochim. Acta.* 281 (2018) 170-188.
- [69]C.-H. Wang, N. Kurra, M. Alhabeb, J.-K. Chang, H. N. Alshareef, Y. Gogotsi, Titanium carbide (MXene) as a current collector for lithium-ion batteries, *ACS Omega* 3 (2018) 12489-12494.
- [70]P. A. Maughan, L. Bouscarrat, V. R. Seymour, S. Shao, S. J. Haigh, R. Dawson, N. Tapia-Ruiz, N. Bimbo, Pillared Mo<sub>2</sub>TiC<sub>2</sub> MXene for high-power and long-life lithium and sodium-ion batteries, *Nanoscale Adv.* 3 (2021) 3145-3158.
- [71]S. Zhao, Z. Liu, G. Xie, X. Guo, Z. Guo, F. Song, G. Li, C. Chen, X. Xie, N. Zhang, B. Sun, S. Guo, G. Wang, Achieving high-performance 3D K(+) -pre-intercalated Ti<sub>3</sub>C<sub>2</sub>Tx MXene for potassium-ion hybrid capacitors via regulating electrolyte solvation structure, *Angew Chem. Int. Ed.* 60 (2021) 26246-26253.
- [72]G. Ma, H. Shao, J. Xu, Y. Liu, Q. Huang, P.-L. Taberna, P. Simon, Z. Lin, Li-ion storage properties of two-dimensional titanium-carbide synthesized via fast one-pot method in air atmosphere, *Nat. Commun.* 12 (2021) 5085.
- [73]C. Huang, Y. Liu, R. Zheng, Z. Yang, Z. Miao, J. Zhang, X. Cai, H. Yu, L. Zhang, J. Shu, Interlayer gap widened TiS<sub>2</sub> for highly efficient sodium-ion storage, *J. Mater. Sci. Technol.* 107 (2022) 64-69.
- [74]H. Tian, Y. He, L. Wang, Y. Lai, J. Wang, H. Xiang, W. Zhao, L. Zhang, Simultaneous pre-intercalation of caesium and sodium ions into vanadium oxide bronze nanowires for high-performance aqueous zinc-ion batteries, *Mater. Chem. Front.* 6 (2022) 1920-1928.
- [75]Y. Xu, X. Deng, Q. Li, G. Zhang, F. Xiong, S. Tan, Q. Wei, J. Lu, J. Li, Q. An, L. Mai, Vanadium oxide pillared by interlayer Mg<sup>2+</sup> ions and water as ultralong-life cathodes for magnesium-ion batteries, *Chem.* 5 (2019) 1194-1209.
- [76]C. N. R. Rao, G. V. Subba Rao, Electrical conduction in metal oxides. *physica status solidi (a)* 1 (1970) 597-652.
- [77]L. Ling, X. Wang, M. Zhou, K. Wu, C. Lin, H. A. Younus, M. Zhang, S. Zhang, F. Cheng, Y. Zhang, Carbon-coated flower-like TiO<sub>2</sub> nanosphere as an ultrastable anode material for potassium-ion batteries: Structure design and mechanism study, *ACS Appl. Energy Mater.* 5 (2022) 15586-15596.
- [78]J. Collins, G. Gourdin, M. Foster, D. Qu, Carbon surface functionalities and SEI formation during Li intercalation, *Carbon* 92 (2015) 193-244.
- [79]J. O. Besenhard, M. Winter, J. Yang, W. Biberacher, Filming mechanism of lithium-carbon anodes in organic and inorganic electrolytes, *J. Power Sources.* 54 (1995) 228-231.
- [80]A. G. Milnes, *Deep impurities in semiconductors*: Wiley-Interscience; 1973.
- [81]Y. P. Sánchez, A. Santos, P. R. Bueno, Quantum mechanical meaning of the charge transfer resistance, *J. Phys. Chem. C* 126 (2022) 3151-3162.

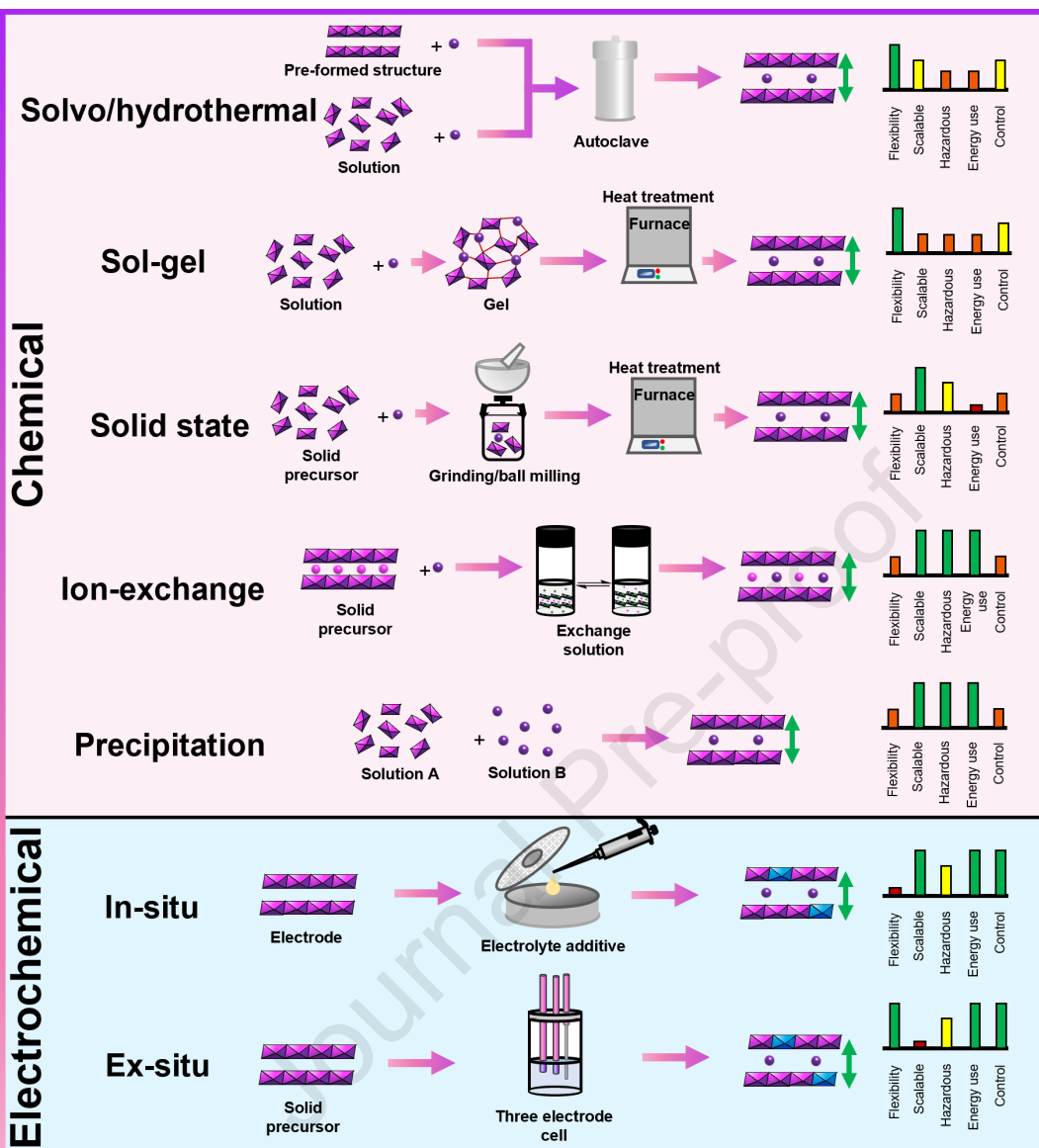
- [82]H. Xia, X. Zhu, J. Liu, Q. Liu, S. Lan, Q. Zhang, X. Liu, J. K. Seo, T. Chen, L. Gu, Y. S. Meng, A monoclinic polymorph of sodium birnessite for ultrafast and ultrastable sodium ion storage, *Nat Commun.* 9 (2018) 5100.
- [83]S. Ding, X. Dai, Y. Tian, B. Song, L. Wang, G. Li, S. Li, J. Huang, Z. Li, A. Meng, Insight into the coordinating mechanism of multi-electron reaction and structural stability induced by K<sup>+</sup> pre-intercalation for magnesium ions batteries, *Nano Energy* 93 (2022) 106838.
- [84]P. He, G. Zhang, X. Liao, M. Yan, X. Xu, Q. An, J. Liu, L. Mai, Sodium ion stabilized vanadium oxide nanowire cathode for high-performance zinc-ion batteries, *Adv. Energy Mater.* 8 (2018) 1702463.
- [85]X. Zhao, L. Mao, Q. Cheng, F. Liao, G. Yang, L. Chen, A new sodium ion preintercalated and oxygen vacancy-enriched vanadyl phosphate cathode for aqueous zinc-ion batteries, *J Colloid Interface Sci.* 627 (2022) 1021-1029.
- [86]X. Zhao, L. Mao, Q. Cheng, F. Liao, G. Yang, L. Chen, Dual-cation preintercalated and amorphous carbon confined vanadium oxides as a superior cathode for aqueous zinc-ion batteries, *Carbon* 186 (2022) 160-170.

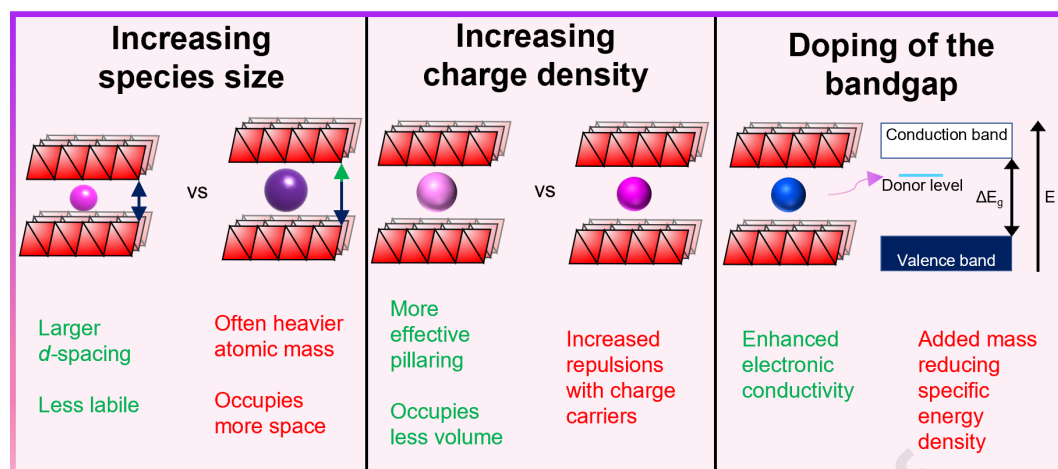
## Graphical Abstract


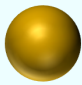


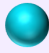
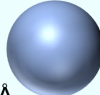
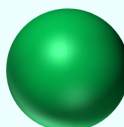
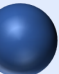

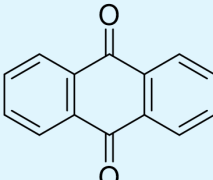
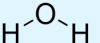



1204

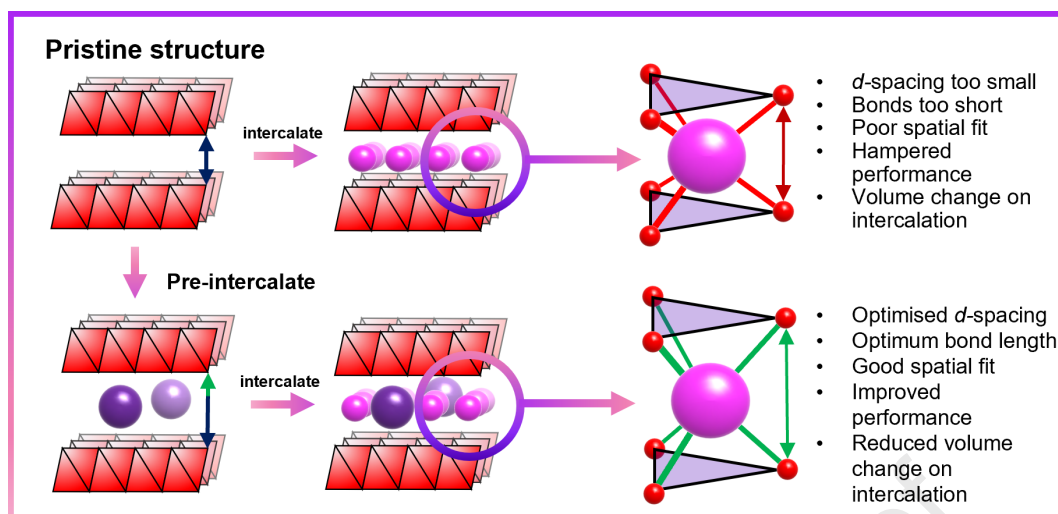


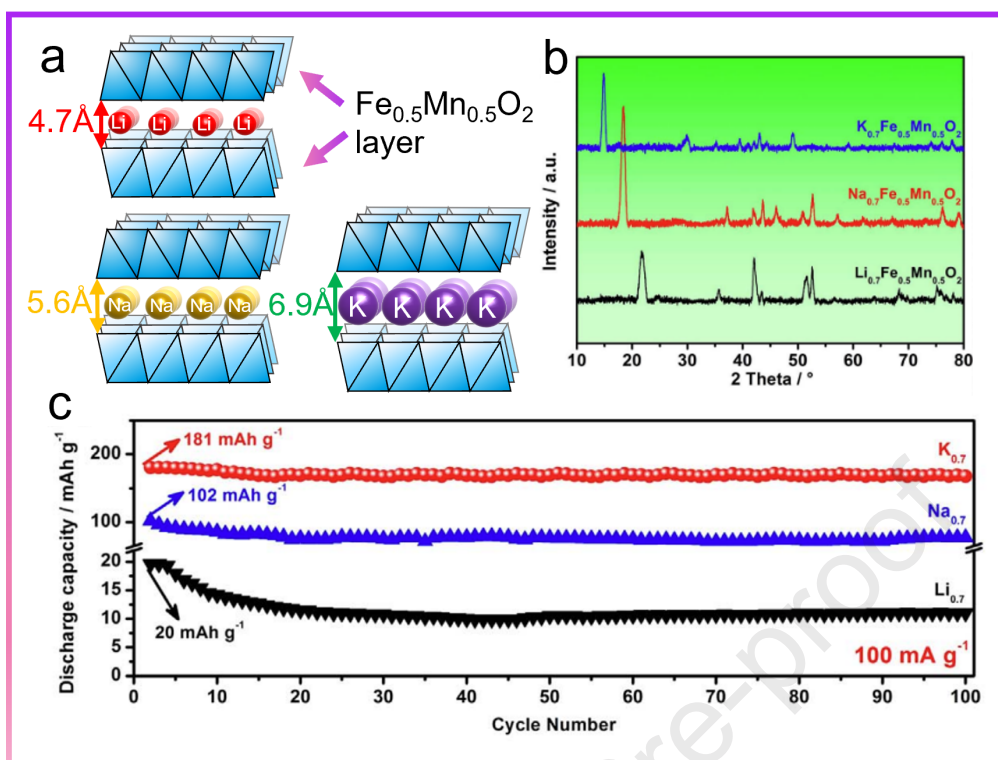


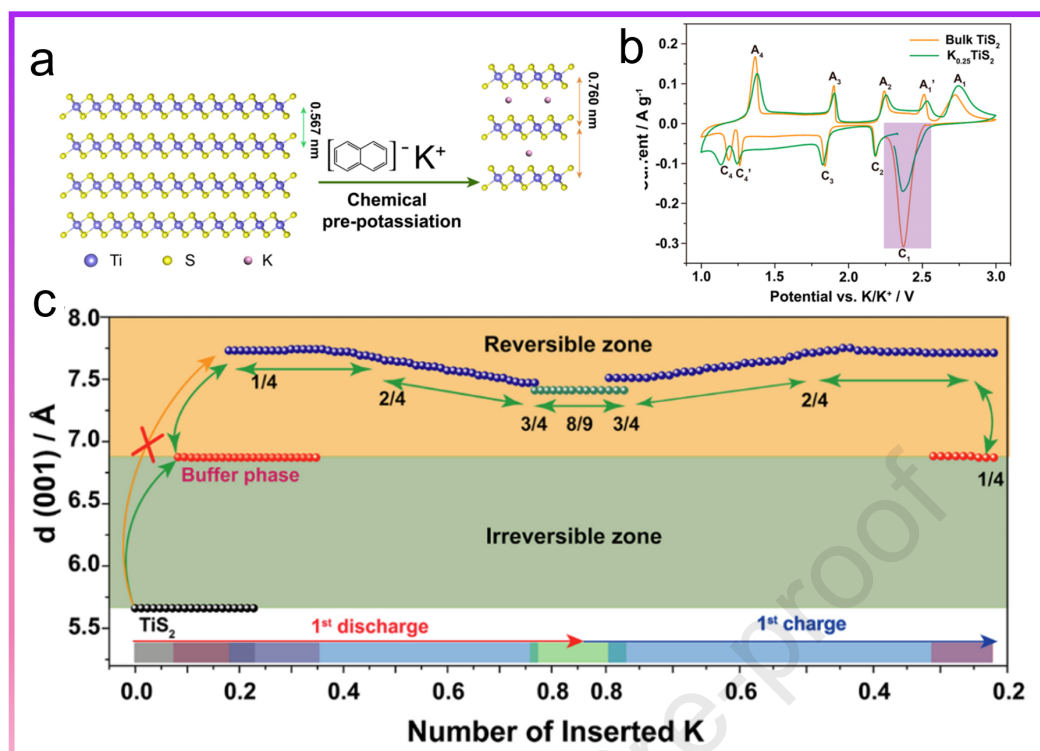


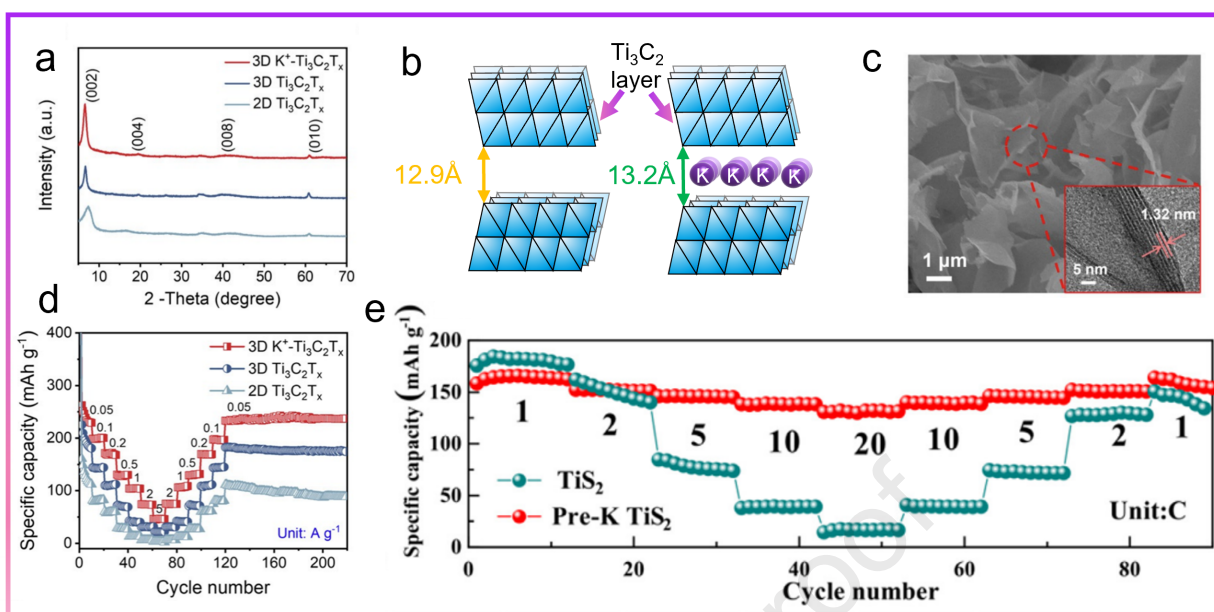
Monovalent			Divalent	Trivalent
$\text{Li}^+$  20 ppm 0.73 Å 52 C mm <sup>-3</sup>	$\text{Na}^+$  23,600 ppm 1.16 Å 24 C mm <sup>-3</sup>	$\text{K}^+$  20,900 ppm 1.43 Å 11 C mm <sup>-3</sup>	$\text{Mg}^{2+}$  23,300 ppm 0.86 Å 52 C mm <sup>-3</sup>	$\text{Al}^{3+}$  82,300 ppm 0.67 Å 364 C mm <sup>-3</sup>
$\text{NH}_4^+$  1.48 Å 11 C mm <sup>-3</sup>	$\text{Cs}^+$  3 ppm 1.88 Å 6 C mm <sup>-3</sup>		$\text{Ca}^{2+}$  41,500 ppm 1.14 Å 120 C mm <sup>-3</sup>	$\text{Y}^{3+}$  33 ppm 1.15 Å 102 C mm <sup>-3</sup>
<div> <div> <div>9.20 Å</div> <div></div> <div>Anthraquinone</div> </div> <div> <div>1.60 Å</div> <div></div> <div>Water</div> </div> <div> <div>4.41 Å</div> <div></div> <div>Benzoquinone</div> </div> </div> <div> <div>5.36 Å</div> <div>0.58 Å</div> <div>5.27 Å</div> </div>				

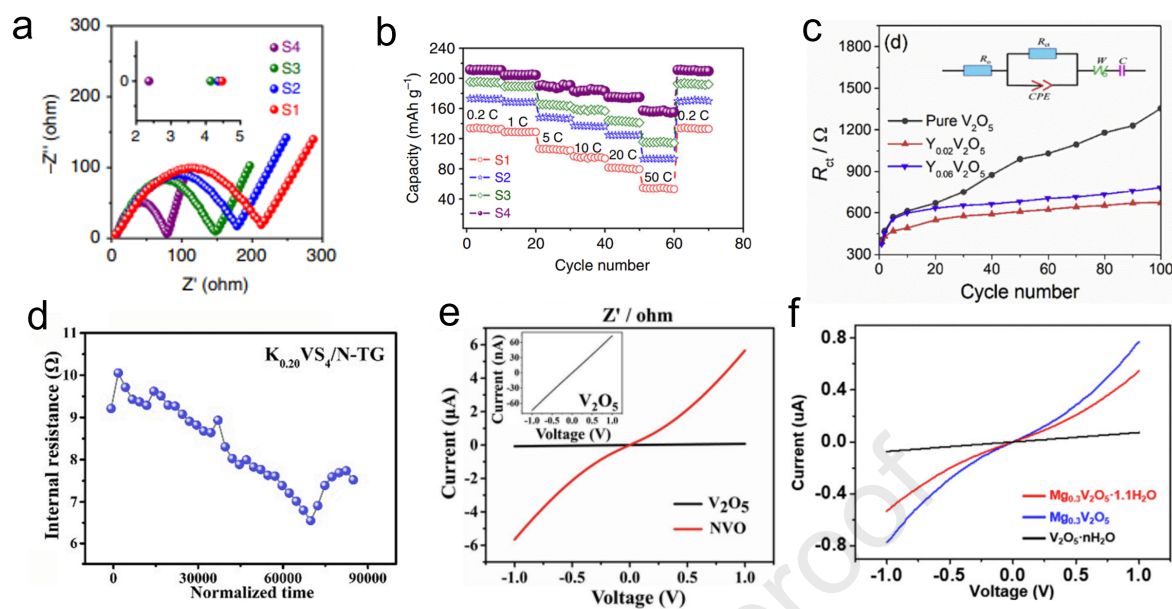












Highlights for Manuscript ESCI-D-22-00058:

- The fundamentals, effects, advantages and pitfalls of pre-intercalation are covered.
- A wide range of materials are reviewed to illustrate and analyse pre-intercalation.
- Perspectives and opinions on the future work in the field are offered.

**Declaration of interests**

☒ The authors declare that they have no known competing financial interests or personal relationships that could have appeared to influence the work reported in this paper.

☐ The authors declare the following financial interests/personal relationships which may be considered as potential competing interests:

--